

Impact of Siberian observations on the optimization of surface CO₂ flux

Jinwoong Kim¹, Hyun Mee Kim¹, Chun-Ho Cho², Kyung-On Boo², Andrew R. Jacobson^{3, 4}, Motoki Sasakawa⁵, Toshinobu Machida⁵, Mikhail Arshinov⁶, and Nikolay Fedoseev⁷

[1]{Department of Atmospheric Sciences, Yonsei University, Seoul, Republic of Korea}

[2]{National Institute of Meteorological Research, Jeju, Republic of Korea}

[3]{Earth System Research Laboratory, National Oceanic and Atmospheric Administration, Boulder, USA}

[4]{Cooperative Institute for Research in Environmental Sciences, University of Colorado, Boulder, USA}

[5]{Center for Global Environmental Research, National Institute for Environment Studies, Tsukuba, Japan}

[6]{V. E. Zuev Institute of Atmospheric Optics, Russian Academy of Sciences, Tomsk, Russia}

[7]{Melnikov Permafrost Institute, Russian Academy of Sciences, Yakutsk, Russia}

Correspondence to: Hyun Mee Kim (khm@yonsei.ac.kr)

Abstract

To investigate the effect of additional CO₂ observations in the Siberia region on the Asian and global surface CO₂ flux analyses, two experiments using different observation dataset were performed for 2000-2009. One experiment was conducted using a data set that includes additional observations of Siberian tower measurements (Japan-Russia Siberian Tall Tower Inland Observation Network: JR-STATION), and the other experiment was conducted using a data set without the above additional observations. The results show that the global balance of the sources and sinks of surface CO₂ fluxes was maintained for both experiments with and without the additional observations. While the magnitude of the optimized surface CO₂ flux

1 uptake and flux uncertainty in Siberia decreased from -1.17 ± 0.93 Pg C yr⁻¹ to -0.77 ± 0.70 Pg
2 C yr⁻¹, the magnitude of the optimized surface CO₂ flux uptake in the other regions (e.g.,
3 Europe) of the Northern Hemisphere (NH) land increased for the experiment with the
4 additional observations, which affect the longitudinal distribution of the total NH sinks. This
5 change was mostly caused by changes in the magnitudes of surface CO₂ flux in June and July.
6 The observation impact measured by uncertainty reduction and self-sensitivity tests shows
7 that additional observations provide useful information on the estimated surface CO₂ flux.
8 The average uncertainty reduction of the Conifer Forest of EB is 29.1% and the average self-
9 sensitivities at the JR-STATION sites are approximately 60% larger than those at the towers
10 in North America. It is expected that the Siberian observations play an important role in
11 estimating surface CO₂ flux in the NH land (e.g., Siberia and Europe) in the future.

12

13 **1 Introduction**

14 The terrestrial ecosystem in the Northern Hemisphere (NH) plays an important role in the
15 global carbon balance (Hayes et al., 2011; Le Quéré et al., 2015). Especially, Siberia is
16 considered to be the one of the largest CO₂ uptake regions and reservoirs due to its forest area
17 (Schulze et al., 1999; Houghton et al., 2007; Tarnocai et al., 2009; Kurganova et al., 2010;
18 Schepaschenko et al., 2011) and its dynamics and interactions with the climate have global
19 significance (Quegan et al., 2011). Therefore, it is important to accurately estimate the surface
20 CO₂ fluxes in this region. For instance, Dolman et al. (2012) estimated terrestrial carbon
21 budget of Russia, Ukraine, Belarus, and Kazakhstan using inventory-based, eddy covariance,
22 and inversion methods and showed that the carbon budgets produced by three methods agree
23 within their uncertainty bounds.

24 To estimate the surface CO₂ flux, atmospheric CO₂ inversion studies are conducted using
25 atmospheric transport models and atmospheric CO₂ observations (Gurney et al., 2002; Peylin
26 et al., 2013). However, prior emission, measurement error of observation, observation
27 operator including model transport, and representative error affect the uncertainty of
28 atmospheric inversion results (Engelen et al., 2002; Berchet et al., 2015a). Along these factors,
29 large uncertainties remain in the estimated surface CO₂ fluxes due to the sparseness of current
30 surface CO₂ measurements assimilated by inverse models (Peters et al., 2010; Bruhwiler et al.,
31 2011). Peylin et al. (2013) performed an intercomparison study of estimated surface CO₂

1 fluxes from 11 different inversion systems. The results showed that the estimated surface CO₂
2 flux uptake in the NH, where the atmospheric CO₂ network is dense, is similar across the
3 inversion systems; meanwhile, the established flux is noticeably different across the inversion
4 systems for the tropics and SH, where the atmospheric CO₂ network is sparse.

5 Regionally, however, the longitudinal breakdown of all the NH sinks appears to be much
6 more variable than the total flux itself. Therefore, additional observations in a sparse CO₂
7 observation network region are necessary to reduce uncertainty in estimating the surface CO₂
8 flux. Maksyutov et al. (2003) showed that additional observations in the Asia region show the
9 largest effect and reduce the uncertainty in the estimated regional CO₂ fluxes for Siberia
10 during 1992-1996 by time-independent synthesis inversion. Chevallier et al. (2010) also
11 argued that an extension of the observation network toward Eastern Europe and Siberia is
12 necessary to reduce uncertainty in estimated fluxes by inversion methods. Despite the
13 necessity of additional observations in this region, only a few atmospheric CO₂ inversion
14 studies have been conducted using observations in this region due to the deficiency of
15 observations (Quegan et al., 2011).

16 Meanwhile, Reuter et al. (2014) and Feng et al. (2016) reported that the European terrestrial
17 CO₂ uptake inferred by the satellite-retrieved dry-air column-average model fraction of CO₂
18 (XCO₂) is larger than that inferred by a bottom-up inventory approach or inverse modeling
19 systems using surface-based in situ CO₂ atmospheric concentrations. Though a broad spatial
20 coverage of XCO₂ from satellite radiance observations provides useful information for
21 inversion systems in quantifying surface CO₂ fluxes at various scales which is not provided
22 by ground-based measurements, the current XCO₂ has low accuracy and regional biases of a
23 few tenths of a ppm, which may hamper the accuracy of estimated surface CO₂ fluxes (Miller
24 et al., 2007; Chevallier et al., 2007). Therefore, in situ observations determined by surface
25 measurements are necessary to more accurately estimate the surface CO₂ flux in the inverse
26 models.

27 To supply additional observations over Siberia to inverse modeling studies, several efforts to
28 observe the atmospheric CO₂ concentrations in Siberia have been conducted. For example, the
29 Max Planck Institute (MPI) operates a tower (since April 2009), preceded by aircraft
30 measurements (from 1998 to 2005 with 12 to 21 day intervals) at Zotino (ZOTTO; 60.75°N,
31 89.38°E) (Lloyd et al., 2002; Winderlich et al. 2010). In addition, the Airborne Extensive
32 Regional Observations in Siberia (YAK-AEROSIB) aircraft campaign in 2006 (Paris et al.,

1 2008) and Trans-Siberian Observation Into the Chemistry of the Atmosphere (TROICA)
2 project (Turnbull et al., 2009) have measured CO₂ and other chemical species. However,
3 except Zotino that has multi-year measurements, these data collected during specific seasons
4 or over only a few years do not provide the long-term CO₂ concentration data necessary to be
5 used as a constraint in the inverse modeling system.

6 The Center for Global Environmental Research (CGER) of the National Institute for
7 Environmental Studies (NIES) of Japan with the cooperation of the Russian Academy of
8 Science (RAS) constructed a tower network called the Japan-Russia Siberian Tall Tower
9 Inland Observation Network (JR-STATION) in 2002 to measure the continuous CO₂ and CH₄
10 concentrations (eight towers in central Siberia and one tower in eastern Siberia) (Sasakawa et
11 al., 2010, 2013). The vertical profile of CO₂ concentrations from the planetary boundary layer
12 (PBL) to the lower free troposphere is also measured by aircraft at one site of the JR-
13 STATION sites (Sasakawa et al., 2010, 2013). Saeki et al. (2013) estimated the monthly
14 surface CO₂ flux for 68 subcontinental regions by using the fixed-lag Kalman smoother and
15 NIES-TM transport model with JR-STATION data. They reported that the inclusion of
16 additional Siberian observation data has an impact on the inversion results showing larger
17 interannual variability over northeastern Europe as well as Siberia, and reduces the
18 uncertainty of surface CO₂ uptake. Meanwhile, Berchet et al. (2015b) estimated regional CH₄
19 fluxes over Siberia in 2010 by using JR-STATION data.

20 CarbonTracker, developed by the National Oceanic and Atmospheric Administration Earth
21 System Research Laboratory (NOAA ESRL) (Peters et al., 2007), is an atmospheric CO₂
22 inverse modeling system that estimates optimized weekly surface CO₂ flux on a 1°×1°
23 horizontal resolution by using the Ensemble Kalman Filter (EnKF). Since the original
24 CarbonTracker release (Peters et al 2007), a series of improvements have been made with
25 subsequent releases. These include increasing the number of sites from which CO₂ data are
26 assimilated, increasing the resolution of atmospheric transport, improving the simulation of
27 atmospheric convection in TM5, and the use of multiple first-guess flux models to estimate
28 dependence on priors. These improvements are documented at <http://carbontracker.noaa.gov>.
29 Several studies have focused on Asia using CarbonTracker (Kim et al., 2012, 2014a, b; Zhang
30 et al., 2014a, b). Schneising et al. (2011) showed that SCanning Imaging Absorption
31 spectroMeter for Atmospheric CHartography (SCIAMACHY) retrieval data indicate a
32 stronger North American boreal forest uptake and weaker Russian boreal forest uptake

1 compared to CarbonTracker within their uncertainties. On the other hand, Zhang et al.
2 (2014b) estimated surface CO₂ fluxes in Asia by assimilating CONTRAIL (Machida et al.,
3 2008) aircraft CO₂ measurements into the CarbonTracker framework. The CONTRAIL
4 measurements include ascending/descending vertical profiles and cruise data below
5 tropopause. The results show that surface CO₂ uptake over the Eurasian Boreal (EB) region
6 slightly increases from -0.96 Pg C yr⁻¹ to -1.02 Pg C yr⁻¹ for the period 2006-2010 when
7 aircraft CO₂ measurements were assimilated. However, the surface measurements data over
8 the EB region are still not used in the study by Zhang et al. (2014b). Using an influence
9 matrix calculation, Kim et al. (2014b) showed that comprehensive coverage of additional
10 observations in an observation sparse region, e.g., Siberia, is necessary to estimate the surface
11 CO₂ flux in these areas as accurately as that obtained for North America in the CarbonTracker
12 framework.

13 In this study, the impact of additional Siberian observations on the optimized surface CO₂
14 flux over the globe and Asian region within CarbonTracker (The version of CarbonTracker
15 used in this study is based on the CarbonTracker 2010 release) are investigated by comparing
16 the results of estimated surface CO₂ fluxes from two experiments with and without Siberian
17 observations. Section 2 presents the methodology including a priori flux data, atmospheric
18 CO₂ observations, and experimental framework. Section 3 presents the results, and Section 4
19 provides a summary and conclusions.

20

21 **2 Methodology**

22 **2.1 Inversion method**

23 CarbonTracker is an inverse modeling system developed by Peters et al. (2007). Optimized
24 surface CO₂ fluxes with a 1°×1° horizontal resolution are calculated as follows:

$$25 \quad F(x, y, t) = \lambda_r \cdot F_{bio}(x, y, t) + \lambda_r \cdot F_{ocn}(x, y, t) + F_{ff}(x, y, t) + F_{fire}(x, y, t), \quad (1)$$

26 where $F_{bio}(x, y, t)$, $F_{ocn}(x, y, t)$, $F_{ff}(x, y, t)$, and $F_{fire}(x, y, t)$ are a priori emissions from the
27 biosphere, the ocean, fossil fuel, and fires. λ_r is the scaling factor to be optimized in the data
28 assimilation process, corresponding to 156 regions around the globe (126 land and 30 ocean
29 regions). In the land, the ecoregions are defined as the combination of 11 land region of
30 Transcom regions (Gurney et al., 2002) with 19 land-surface characterization based on Olson

1 et al. (1992). Inappropriate combinations of TransCom regions and Olson types are excluded.
 2 In the ocean, 30 ocean regions are defined following Jacobson et al. (2007). The scaling factor
 3 spans 5 weeks with 1 week resolution. Several previous studies for CarbonTracker (e.g.,
 4 Peters et al., 2007; 2010, Kim et al., 2012, 2014a, b; Zhang et al., 2014a, b; van der Laan-
 5 Luijkx et al., 2015) showed that 5 weeks of lag and 1-week time resolution are appropriate for
 6 optimizing the surface CO₂ fluxes. In each assimilation cycle (i.e., analysis step), the entire
 7 scaling factor for 5 weeks is updated by 1 week observations measured most recent week by a
 8 time stepping approach. The smoother window moves forward by 1 week at each assimilation
 9 cycle. After 5 assimilation cycles, the first part of the scaling factor analyzed by 5 weeks
 10 observations is regarded as the optimized scaling factor. The more detailed information of the
 11 assimilation process can be found in Kim et al. (2014b).

12 The ensemble Kalman filter (EnKF) data assimilation method used in CarbonTracker is the
 13 ensemble square root filter (EnSRF) suggested by Whitaker and Hamill (2002). The analysis
 14 equation for data assimilation is expressed as

$$15 \quad \mathbf{x}^a = \mathbf{K}\mathbf{y}^o + (\mathbf{I}_n - \mathbf{K}\mathbf{H})\mathbf{x}^b, \quad (2)$$

16 where \mathbf{x}^a is the n-dimensional analysis (posterior) state vector ; \mathbf{y}^o is the p-dimensional
 17 observation vector (atmospheric CO₂ observations); \mathbf{K} is the $n \times p$ dimensional Kalman gain;
 18 \mathbf{I}_n is the identity matrix; \mathbf{H} is the linearized observation operator, which transforms the
 19 information in the model space to the information in the observation space; and \mathbf{x}^b is the
 20 background state vector. In CarbonTracker, the state vector corresponds to the scaling factor.
 21 The Kalman gain \mathbf{K} is defined as

$$22 \quad \mathbf{K} = (\mathbf{P}^b \mathbf{H}^T) (\mathbf{H} \mathbf{P}^b \mathbf{H}^T + \mathbf{R})^{-1}, \quad (3)$$

23 where \mathbf{P}^b is the background error covariance; \mathbf{R} is the observation error covariance or model
 24 data mismatch, which is predefined at each observation site. $\mathbf{P}^b \mathbf{H}^T$ and $\mathbf{H} \mathbf{P}^b \mathbf{H}^T$ in Eq. (3) can
 25 be calculated as

$$26 \quad \mathbf{P}^b \mathbf{H}^T \approx \frac{1}{m-1} (\mathbf{x}'_1, \mathbf{x}'_2, \dots, \mathbf{x}'_m) \cdot (\mathbf{H}\mathbf{x}'_1, \mathbf{H}\mathbf{x}'_2, \dots, \mathbf{H}\mathbf{x}'_m)^T, \quad (4)$$

$$27 \quad \mathbf{H} \mathbf{P}^b \mathbf{H}^T \approx \frac{1}{m-1} (\mathbf{H}\mathbf{x}'_1, \mathbf{H}\mathbf{x}'_2, \dots, \mathbf{H}\mathbf{x}'_m) \cdot (\mathbf{H}\mathbf{x}'_1, \mathbf{H}\mathbf{x}'_2, \dots, \mathbf{H}\mathbf{x}'_m)^T, \quad (5)$$

1 where m is the number of ensembles and $'$ denotes the perturbation of ensemble mean.

2 To reduce the sampling error and filter divergence due to the underestimation of background
3 error covariance in the EnKF, the covariance localization method is used (Houtekamer and
4 Mitchell, 2001). The localization is not applied to Marine Boundary Layer (MBL) sites (e.g.
5 observation sites in Antarctica), because the MBL sites are considered as including
6 information on large footprints of flux signals (Peters et al., 2007). The physical distance
7 between the scaling factors cannot be defined. Therefore, localization is performed based on
8 the linear correlation coefficient between the ensemble of the scaling factor and the ensemble
9 of the model CO₂ concentration (Peters et al., 2007). Statistical significance test is performed
10 on the linear correlation coefficient with a cut-off at a 95% significance in a student's T-test.
11 Then the components of Kalman gain with an insignificant statistical value are set to zero.
12 After one analysis step is completed, the new mean scaling factor that serves as the
13 background scaling factor for next analysis cycle is predicted as

$$14 \quad \lambda_t^b = \frac{(\lambda_{t-2}^a + \lambda_{t-1}^a + 1)}{3}, \quad (6)$$

15 where λ_t^b is a prior mean scaling factor of the current analysis cycle, λ_{t-2}^a and λ_{t-1}^a are
16 posterior mean scaling factors of previous cycles. Eq. (6) propagates information from one
17 step to the next step (Peters et al., 2007).

18 The detailed algorithm of inversion method used in this study can be found in Peters et al.
19 (2007) and Kim et al. (2014a).

20 **2.2 A priori flux data**

21 Four types of a priori and imposed CO₂ fluxes used in this study are as follows: (1) First guess
22 biosphere flux from the Carnegie–Ames–Stanford Approach Global Fire Emissions Database
23 (CASA GFED) version 3.1 (van der Werf et al., 2010). The 3 hour interval Net Ecosystem
24 Exchange (NEE) is calculated from monthly mean Net Primary Production (NPP) and
25 ecosystem respiration (RE) by using a simple temperature Q₁₀¹ relationship and a linear

¹ It is calculated as $Q_{10}(t) = 1.5^{((T_{2m} - T_0)/10.0)}$, where t is time, T_{2m} is temperature (K) at 2 m, and T_0 is 273.15 K.

1 scaling of photosynthesis with solar radiation (Olsen and Randerson, 2004); (2) the prior
2 ocean flux from air-sea partial pressure differences based on Jacobson et al. (2007). Short-
3 term flux variability is derived from the atmospheric model wind speeds via the gas transfer
4 coefficient; (3) biomass burning emissions obtained from GFED v3.1 (van der Werf et al.,
5 2010); (4) the prescribed fossil fuel emission from the Carbon Dioxide Information and
6 Analysis Center (CDIAC, Boden et al., 2010) and the Emission Database for Global
7 Atmospheric Research (EDGAR, European Commission, 2009) databases. The annual global
8 total fossil fuel emissions are based on CDIAC. Fluxes at $1^{\circ} \times 1^{\circ}$ resolution are spatially
9 distributed according to the EDGAR inventories.

10 **2.3 Atmospheric CO₂ observations**

11 Atmospheric CO₂ mole fraction observations measured at surface observation sites are used in
12 this study. Figure 1 shows the observation network and Table 1 presents observation site
13 information for the Asian and European regions. Three sets of atmospheric CO₂ observations
14 data are assimilated: (1) surface CO₂ observations distributed by the NOAA ESRL
15 (observation sites operated by NOAA, Environment Canada (EC), the Australian
16 Commonwealth Scientific and Industrial Research Organization (CSIRO), the National
17 Center for Atmospheric Research (NCAR), and Lawrence Berkeley National Laboratory
18 (LBNL)) (observation data is available at [http://www.esrl.noaa.gov/gmd/ccgg/obspack/
19 data.php](http://www.esrl.noaa.gov/gmd/ccgg/obspack/data.php); Masarie et al., 2014); (2) World Data Centre for Greenhouse Gases (WDCGG,
20 <http://ds.data.jma.go.jp/wdcgg/>); (3) JR-STATION observation data over Siberia operated by
21 CGER/NIES (Sasakawa et al., 2010, 2013). The JR-STATION sites consist of nine towers
22 (eight towers in west Siberia and one tower in east Siberia). Atmospheric air was sampled at
23 four levels on the BRZ tower and at two levels on the other eight towers. At the BRZ
24 (Berezorechka) site in west Siberia, both tower and aircraft measurements are sampled. The
25 light aircraft at BRZ site measures the vertical profiles of CO₂ from the PBL to the lower free
26 troposphere and these vertical profiles are used as independent observations for verification.

27 Sampled CO₂ data were calibrated against the NIES 09 CO₂ scale which are lower than the
28 WMO-X2007 CO₂ scale by 0.07 ppm at around 360 ppm and consistent in the range between
29 380 and 400 ppm (Machida et al., 2011). Detailed description of JR-STATION sites can be
30 found in Sasakawa et al. (2010, 2013). Daytime averaged CO₂ concentrations (1200-1600
31 LST, representing the time when active vertical mixing occurred in the PBL) for each day

1 from the time series at the highest level of tower measurements are used in the data
2 assimilation.

3 In CarbonTracker, model data mismatch (MDM, \mathbf{R} in Eq. (7)) is assigned by site categories.
4 The location of each observation site is represented in Fig. 1. The assigned MDM requires
5 innovation χ^2 statistics in Eq. (7) become close to one at each observation site (Peters et al.
6 2007).

$$7 \quad \chi^2 = \frac{(\mathbf{y}^o - \mathbf{H}\mathbf{x}^b)^2}{\mathbf{H}\mathbf{P}^b\mathbf{H}^T + \mathbf{R}}, \quad (7)$$

8 where $\mathbf{y}^o - \mathbf{H}\mathbf{x}^b$ represent innovation. The site categories and MDM values are assigned the
9 same value as in previous studies (Peters et al., 2007; Kim et al. 2014b; Zhang et al., 2014b):
10 marine boundary layer (0.75 ppm), continental sites (2.5 ppm), mixed land/ocean and
11 mountain sites (1.5 ppm), continuous sites (3.0 ppm), and difficult sites (7.5 ppm).
12 Continuous site category is generally used for observations measured continuously. For the
13 JR-STATION sites that have continuous tower measurements, the MDM is set to 3 ppm,
14 which is the same as tower measurements in North America.

15 **2.4 Experimental framework**

16 Two experiments with different set of observations are conducted in this study: one
17 experiment, the CNTL experiment, is conducted by using set of observations without
18 observations in the Siberia region (black color observation sites represented in Fig. 1); the
19 other experiment, the JR experiment, is conducted by using all available observations
20 including the Siberia data (all observation sites represented in Fig. 1). The TM5 model (Krol
21 et al., 2005) which calculates four-dimensional CO₂ concentration field runs at global 3°×2°
22 horizontal resolution and a nesting domain centered in Asia with 1°×1° horizontal resolution.
23 The nesting domain is shown in Fig. 1. Meteorological variables for running the TM5
24 transport model are from the European Centre for Medium-Range Weather Forecasts
25 (ECMWF) forecast model output. The experimental period is from 1 January 2000 to 31
26 December 2009. The observation data commonly used for CNTL and JR experiments exist
27 from 2000, but the additional Siberia data for the JR experiment exist from 2002. The number
28 of ensembles is 150, and the scaling factor includes 5 weeks of lag, as in previous studies
29 (Peters et al., 2007, 2010; Peylin et al., 2013; Kim et al., 2012, 2014a b; Zhang et al., 2014a,
30 b).

1

2 **3 Results**

3 **3.1 Characteristics of carbon fluxes**

4 In this section, optimized surface CO₂ fluxes inferred from the two experiments are examined.
5 The optimized surface CO₂ flux in 2000 and 2001 is excluded from this analysis because
6 2000 is considered a spin-up year similar to previous studies using CarbonTracker, and JR-
7 STATION data are used since 2002. Only the biosphere and ocean fluxes are presented here
8 because fires (biomass burning) and fossil fuel emissions are not optimized in CarbonTracker.

9 Figure 2 presents the spatial distribution of the averaged prior and optimized biosphere and
10 ocean fluxes of the two experiments and the difference between the CNTL and JR
11 experiments from 2002 to 2009. The optimized biosphere flux uptakes of the CNTL and JR
12 experiments are globally 1.60 ~ 1.61 Pg C yr⁻¹ greater than the prior flux uptakes (Figs. 2a, c,
13 d, Table 2). The difference in fluxes between the prior and JR experiment is large in EB (Figs.
14 2a, d) although smaller than that between the prior and CNTL experiment (Figs. 2a, c). The
15 differences in fluxes between the CNTL and JR experiments are distinctive in EB (Siberia)
16 where the new additional observations are assimilated (Fig. 2b). The magnitude of surface
17 CO₂ uptakes decreases in that region by assimilating JR-STATION observation data. On the
18 contrary, the average surface CO₂ uptakes in other regions, such as North America, Europe,
19 the western North Pacific Ocean, and the Atlantic Ocean, increase by assimilating JR-
20 STATION observation data.

21 The difference in the optimized CO₂ flux between the two experiments is analyzed. Table 2
22 presents prior and optimized fluxes with their uncertainties for global total, global land, global
23 ocean, NH total, Tropics total, Southern Hemisphere total, and TransCom regions in the NH.
24 Flux uncertainties are calculated from the ensembles of prior and optimized surface fluxes
25 assuming Gaussian errors, following previous method used in Peters et al. (2007, 2010). The
26 global total biogenic and oceanic optimized CO₂ fluxes are similar for each experiment at -
27 5.54±1.85 Pg C yr⁻¹ (CNTL experiment) and -5.55±1.72 Pg C yr⁻¹ (JR experiment), compared
28 with the global prior flux of -3.94±2.24 Pg C yr⁻¹. The global land sink in the CNTL
29 experiment is larger by 0.07 Pg C yr⁻¹ than that of the JR experiment, and the global ocean
30 sink in the CNTL experiment is smaller by 0.08 Pg C yr⁻¹ than that of the JR experiment. The
31 additional observations do not make any discrepancy between the two experiments with

1 respect to the global total sink, and they indicate only a small difference in the land-ocean
2 CO₂ flux partitioning. The estimated CO₂ flux uncertainty in the land region from the JR
3 experiment is smaller than that of the CNTL experiment because new observations provide
4 additional constraints on the optimized CO₂ flux. For specific regions in the NH, a large
5 difference of optimized surface CO₂ flux is observed in the EB. The largest increment
6 between a priori and CNTL is shown in EB with the least in situ observations as shown in Fig.
7 1. The other regions show smaller increment with more ‘local’ observations available. The
8 surface CO₂ uptakes in the EB of the CNTL experiment is -1.17 ± 0.93 Pg C yr⁻¹ and that of the
9 JR experiment is -0.77 ± 0.70 Pg C yr⁻¹, respectively. The uncertainty of the optimized surface
10 CO₂ uptake in the EB in the JR experiment is expectedly reduced by assimilating additional
11 observations. In contrast, the surface CO₂ uptake increases in other regions of the NH.

12 Figure 3 presents the spatial distribution of the optimized biosphere fluxes difference between
13 the CNTL and JR experiments from 2002 to 2009. The difference of optimized surface CO₂
14 flux is calculated as in Fig. 2b. The largest difference of optimized surface CO₂ fluxes
15 between the two experiments occurs in Siberia. The uptake of optimized surface CO₂ flux in
16 this region is reduced in JR for all years except 2003. In 2003, extreme drought occurred in
17 the northern mid-latitudes (Knorr et al., 2007) and Europe (Ciais et al., 2005), which resulted
18 in increased NEE (i.e. reduced uptake of CO₂) in EB in the CNTL experiment. The uptake of
19 optimized surface CO₂ fluxes in Siberia in 2003 is reduced in the CNTL experiment due to
20 the remote effect of drought in Europe. Despite the number of JR-STATION data used in the
21 optimization in 2003 being relatively smaller than that in the later experiment period, new
22 observations in the JR experiment provide information on the increased uptake of optimized
23 surface CO₂ fluxes in 2003 in Siberia (Fig. 3b).

24 Optimized surface CO₂ fluxes averaged from 2002 to 2009 for each ecoregion in the NH are
25 shown in Table 3. In the Siberia (EB), optimized surface CO₂ uptake from the JR experiment
26 is smaller (larger) than that of the CNTL experiment in the Conifer Forest and Northern Taiga
27 (in other ecoregions). In the Eurasian Temperate (ET), Europe, North American Boreal
28 (NAB), and North American Temperate (NAT) regions, the optimized surface CO₂ uptakes
29 from the JR experiment are larger than those of the CNTL experiment in most ecoregions.

30 Figure 4 shows the time series of annual and average prior and optimized surface CO₂ fluxes
31 over global total, global land, and global ocean. For global total, the magnitude of optimized
32 fluxes are much greater than that of prior fluxes due to the greater uptake of optimized fluxes

1 than that of prior fluxes over global land (Figs. 4a and b). In contrast, the magnitude of
2 optimized fluxes over global ocean is slightly weaker than that of prior fluxes (Fig. 4c). As
3 shown in Table 2, the differences between annual and average optimized surface CO₂ fluxes
4 over the globe are small and the average is almost the same for the two experiments (Fig. 4a)
5 with a similar trend of -0.33 Pg C yr⁻² and -0.35 Pg C yr⁻² in CNTL and JR experiment
6 respectively, and the differences in global land and ocean are also small (Figs. 4b, c) with a
7 similar trend of -0.22 Pg C yr⁻² in global land of both CNTL and JR experiment and -0.11 Pg
8 C yr⁻² and -0.13 Pg C yr⁻² in global ocean of CNTL and JR experiment respectively. The
9 optimized surface CO₂ fluxes from each experiment show similar interannual variability,
10 which implies that the additional Siberian observations do not affect the interannual
11 variability of global surface CO₂ uptakes.

12 Figure 5 is the same as Fig. 4 but covers land regions in the NH. Although the optimized
13 surface CO₂ fluxes over global total are similar, those over each TransCom region are
14 different in each experiment. The optimized fluxes over each region show greater annual
15 uptake relative to the prior fluxes in both experiment. The difference between the two
16 experiments is largest in the EB as expected (Fig. 5a). The JR experiment exhibits a weaker
17 surface CO₂ uptake in the EB than does the CNTL experiment except for 2003 as shown in
18 Fig. 3b, whereas the JR experiment exhibits a greater surface CO₂ uptake in the other regions,
19 especially over Europe in 2008 and 2009, than the CNTL experiment (Figs. 5b, c, d, and e). It
20 is driven by the increase of CO₂ uptake in Eastern Europe (Figs. 3g and h). Because most of
21 JR-STATION sites are located in the western part of Siberia (Fig. 1), the optimized surface
22 CO₂ fluxes over Eastern Europe could be affected by JR-STATION observations. The trend
23 of EB in CNTL experiment is -0.06 Pg C yr⁻², whereas that in JR experiment is 0.02 Pg C yr⁻²
24 due to the reduced uptake of CO₂ in JR experiment since 2005 (Fig 5a). As a result, the trends
25 of the surface CO₂ uptake of EB and Europe in two experiments show opposite signs. In
26 contrast, the surface CO₂ uptake trends of other land regions in NH are similar between the
27 two experiments.

28 Figure 6 shows monthly prior and optimized surface CO₂ fluxes averaged from 2002 to 2009
29 with their uncertainties from both experiments. In general, optimized fluxes in both
30 experiments show greater uptake in boreal summer and weaker uptake in other seasons
31 compared to the prior fluxes, which results in greater annual CO₂ uptake of optimized fluxes
32 than prior fluxes as shown in Fig. 5. The largest difference in surface CO₂ flux between the

1 two experiments occurs in June and July, which represent the active season of the terrestrial
2 ecosystem with a large surface CO₂ flux uncertainty. The JR experiment exhibits a weaker
3 surface CO₂ summer uptake in the EB (Fig. 6a) and slightly greater uptake in the other
4 regions (Figs. 6b, c, d, and e). These additional JR-STATION data provides information on
5 the surface CO₂ uptake by vegetation activities in the NH summer.

6 **3.2 Comparison with observations**

7 Table 4 presents the average bias of the model CO₂ concentrations calculated by the
8 background and optimized fluxes of the two experiments at each observation site located in
9 Asia and Europe from 2002 to 2009. The bias is calculated by subtracting the observed CO₂
10 concentrations from the model CO₂ concentrations. Biases of the JR experiment are smaller
11 than those of the CNTL experiment at the JR-STATION sites, which indicates that the
12 optimized surface CO₂ flux of the JR experiment is more consistent with the observed CO₂
13 concentrations than that in the CNTL experiment. The negative bias at five JR-STATION
14 sites (DEM, IGR, KRZ, NOY, and YAK) located in the forest area of the EB is reduced
15 compared with those of the CNTL experiment, which indicates that the optimized surface
16 CO₂ uptake of the CNTL experiment is overestimated with respect to CO₂ concentration
17 observations in Siberia. Otherwise, the reduced surface CO₂ uptake of the JR experiment
18 exhibits more consistent model CO₂ concentrations in this region. In addition to the average
19 bias for the entire period, the time series of monthly averaged bias of the model CO₂
20 concentration from the observed CO₂ concentration at JR-STATION sites shows that the JR
21 experiment consistently shows smaller biases compared to the CNTL experiment (not shown),
22 which implies that the model representation of CO₂ at JR-STATION sites is more accurate in
23 the JR experiment than in the CNTL experiment. Model CO₂ concentrations calculated by
24 background surface CO₂ fluxes in the JR experiment are also more consistent with the
25 observations, implying that background scaling factors of the JR experiment are more
26 accurate than those of the CNTL experiment. The background surface CO₂ fluxes are
27 calculated by multiplying the background scaling factor to prior biosphere and ocean fluxes as
28 in Eq. (1). In addition, the average innovation χ^2 -statistics at the JR-STATION sites are
29 generally close to 1, implying that the defined MDM is an appropriate value. Therefore, by
30 assimilating JR-STATION observation data, the JR experiments exhibits better results than
31 the CNTL experiment at observation sites in EB.

1 However, at observation sites in ET and Europe, the difference in biases of the two
2 experiments is relatively small and not significant enough to determine which experiment
3 exhibits better results. This is due to the small difference of optimized surface CO₂ fluxes
4 between the two experiments in the ET region. The observation sites in Europe are located far
5 from Eastern Europe and Siberia as shown in Fig. 1 so that they are not sensitive to the
6 change of surface CO₂ uptake in those regions. In addition, the MDM at four sites (BAL, BSC,
7 HUN, and OBN) in Europe is assigned as 7.5 ppm, the largest value in CarbonTracker, due to
8 poor representation of the transport model at these sites (Peters et al., 2010).

9 In addition, model CO₂ concentrations calculated by optimized fluxes of the two experiments
10 are compared with independent, not assimilated, vertical profiles of CO₂ concentration
11 measurements by aircraft at BRZ site in Siberia. Table 5 presents the average bias, root-mean-
12 square difference (RMSD), mean absolute error (MAE), and Pearson's correlation coefficient
13 of the model CO₂ concentrations calculated by optimized fluxes of the two experiments based
14 on the observations at BRZ site as the reference. The statistics are calculated at each vertical
15 bin with 500 meter interval. Overall, the biases of two experiments are less than 0.83 ppm
16 showing good consistency between model and observed CO₂ concentrations. The biases of
17 the CNTL experiment are smaller than those of the JR experiment at all altitudes, whereas the
18 standard deviations of the CNTL experiment are greater than those of JR experiment, which
19 implies that the biases of the CNTL experiment fluctuate as its average more than those of the
20 JR experiment. In contrast, the RMSD and MAE of the JR experiment are smaller than those
21 of the CNTL experiment, and the correlation coefficient of the JR experiment is greater than
22 that of the CNTL experiments. Therefore, overall the statistics show that the model CO₂
23 concentrations of the JR experiment is relatively more consistent with independent CO₂
24 concentration observations compared to those of the CNTL experiment over Siberia.

25 **3.3 Uncertainty reduction and observation impact**

26 The effects of additional observations on the optimized surface CO₂ flux and associated
27 uncertainties are investigated. Figure 7 shows the average, average in summer (June, July, and
28 August) and average in winter (December, January, February) uncertainty reductions from
29 2002 to 2009. The uncertainty reduction based on the uncertainty of CNTL as the reference is
30 calculated as

$$1 \quad UR = \frac{\sigma_{CNTL} - \sigma_{JR}}{\sigma_{CNTL}} \times 100(\%), \quad (8)$$

2 where σ_{CNTL} and σ_{JR} are one-sigma standard deviations of the optimized scaling factor for
3 CNTL experiment and JR experiment, respectively, assuming Gaussian errors. The maximum
4 uncertainty reduction is the greatest value in any week in the period 2002 to 2009 in each
5 ecoregion. As expected, the average uncertainty reduction is readily apparent in the Conifer
6 Forest of EB in which JR stations are mainly located, which has the additional observations
7 (Fig. 7a). The uncertainty reduction of Asia and Europe, especially in the forest of Siberia and
8 Eastern Europe, is greater than for other regions. The spatial pattern of the maximum
9 uncertainty reduction is similar to that of the average values (not shown). The uncertainty
10 reduction of EB in summer is higher than that in winter (Figs. 7b, c) due to a higher
11 uncertainty associated with larger net fluxes in summer compared to winter (Fig. 6a). For
12 example, the average value of the Conifer Forest of EB is 29.1%, the maximum value is
13 78.6%, the average value in summer is 36.3% and the average value in winter is 29.7%,
14 respectively. The uncertainty reduction of CNTL and JR experiments based on the prior
15 uncertainty as the reference (σ_{prior} used instead of σ_{CNTL} in Eq. (8); σ_{CNTL} or σ_{JR} used instead
16 of σ_{JR} in Eq. (8)) shows similar values in the NH except in Siberia region (not shown). In
17 addition, the difference between average uncertainty reduction of CNTL and JR experiments
18 based on the prior uncertainty as the reference (not shown) is very similar to the average of
19 uncertainty reduction in Eq. (8) shown in Fig. 7a. Therefore, the uncertainties of the optimized
20 surface CO₂ fluxes are reduced by the additional observations.

21 To investigate the impact of individual observations on the optimized surface CO₂ flux, the
22 self-sensitivities are calculated by the method demonstrated by Kim et al. (2014b). The self-
23 sensitivity is the diagonal element of the influence matrix which measures the impact of
24 individual observations in the observation space on the optimized surface CO₂ flux. The large
25 self-sensitivity value implies that the information extracted from observations is large. Figure
26 8 shows the self-sensitivities of the two experiments averaged from 2002 to 2009. The
27 average self-sensitivities at the JR-STATION sites are approximately 60% larger than those at
28 the towers in North America, i.e., continuous site category observations in Fig. 1. The global
29 average self-sensitivities are 4.83% (CNTL experiment) and 5.08% (JR experiment), and the
30 cumulative impacts for the 5 weeks assimilation window are 18.79% (CNTL experiment) and
31 19.33% (JR experiment). The average self-sensitivities of additional observations are higher

1 than those of other sites, providing much information for estimating surface CO₂ fluxes. In
2 particular, YAK site located in east Siberia provides greater impacts than other JR-STATION
3 sites located in 60 ~ 90°E.

4 The RMSDs between the optimized surface CO₂ fluxes and the background fluxes at each
5 assimilation step in summer are calculated (Fig. 9). The RMSD of the analyzed surface CO₂
6 fluxes constrained by one week of observations from the background fluxes in JR experiment
7 is greater than that in CNTL experiment (Figs. 9a, b), implying that surface CO₂ fluxes in
8 Siberia are analyzed by JR-STATION data in Siberia directly at the first cycle. This is
9 consistent with the high value of self-sensitivities at JR-STATION sites as shown in Fig. 8b.
10 Because JR-STATION data are abundant and have large self-sensitivities, these observations
11 provide large information on the estimated surface CO₂ fluxes over Siberia in the first cycle.
12 Kim et al. (2014b) showed that the RMSD in Asia increases after 5 weeks of optimization,
13 which implies that it takes more than 1 week to affect the surface CO₂ fluxes in Siberia by the
14 transport of the CO₂ concentrations observed in remote regions. However, by assimilating the
15 CO₂ concentrations observed at the JR-STATION sites in Siberia, the observation impact on
16 the optimized surface CO₂ fluxes in Siberia increases after 1 week of optimization (Fig. 9b).
17 In contrast, the RMSD in the Siberia region increases after 5 weeks of optimization in the
18 CNTL experiment compared to that in the JR experiment (Figs. 9c, d), which corresponds to
19 the reduced uptake of optimized surface CO₂ fluxes in JR experiment as shown in Fig. 2b.

20 **3.4 Comparison with other results**

21 A comparison of the optimized surface CO₂ flux in this study with other previous studies is
22 presented in Table 6. In the EB, the land sink from the JR experiment (-0.77 ± 0.70 Pg C yr⁻¹)
23 is smaller than those reported by Zhang et al. (2014b) (-1.02 ± 0.91 Pg C yr⁻¹), Maki et al.
24 (2010) (-1.46 ± 0.41 Pg C yr⁻¹), and the CT2013B (CarbonTracker released on 9 February
25 2015; documented online at <http://www.esrl.noaa.gov/gmd/ccgg/carbontracker/CT2013B/>)
26 results (-1.00 ± 3.75 Pg C yr⁻¹), but higher than those reported by Saeki et al. (2013) ($-$
27 0.35 ± 0.61 Pg C yr⁻¹; including biomass burning 0.11 Pg C yr⁻¹), and similar with those
28 reported by Dolman et al. (2012) (-0.613 Pg C yr⁻¹).

29 Because CT2013B and Zhang et al. (2014b) use the similar inversion framework as this study,
30 the reduced land sink is caused by assimilating additional observations. The difference in land
31 sink between the JR experiment and Saeki et al. (2013) is caused by a different inversion

1 system framework which includes prior flux information, atmospheric transport model,
2 observation data set, and inversion method. Despite different inversion system framework
3 used in each study, two studies using the JR-STAITON data exhibit similar results in relative
4 terms, reduced uptake of CO₂ fluxes and uncertainties over Siberia. Nonetheless, the land sink
5 from the JR experiment is somewhat different with other inversion results, its value falls
6 within the flux uncertainty range. Although the land sink in Dolamn et al. (2012) is the
7 average land sink obtained from three methods (inventory-based, eddy covariance, and
8 inversion methods) and estimated not only for Siberia but for Russian territory including
9 Ukraine, Belarus, and Kazakhstan, the land sinks of the JR experiment and Dolman et al.
10 (2012) shows similar values. Overall, the optimized surface CO₂ fluxes in EB of JR
11 experiment are comparable to those of other previous studies.

12 In Europe, though the long-term average land sink from the JR experiment (-0.37 ± 0.64 Pg C
13 yr^{-1}) is higher than that of CTE2014 (-0.07 ± 0.49 Pg C yr^{-1}), the average land sink from 2008-
14 2009 of the JR experiment (-0.75 ± 0.63 Pg C yr^{-1}) is much higher than that of CTE2014 ($-$
15 0.11 ± 0.38 Pg C yr^{-1}). The land sinks of the JR experiment in 2008 and 2009 are -0.73 ± 0.41
16 and -0.76 ± 0.38 Pg C yr^{-1} , respectively, whereas much lower uptakes (-0.21 ± 0.49 , -0.38 ± 0.44
17 Pg C yr^{-1}) are obtained for the CNTL experiment. According to Reuter et al. (2014), despite
18 the different experiment period, the land sink of Europe in 2010 (-1.02 ± 0.30 Pg C yr^{-1})
19 estimated by using satellite observations is much higher than previous inversion studies (e.g.,
20 Peylin et al. 2013) using only surface observations.

21

22 **4 Summary and conclusions**

23 In this study, to investigate the effect of the Siberian observations, which are not used in the
24 previous studies using CarbonTracker, on the optimization of surface CO₂ fluxes, two
25 experiments, named CNTL and JR, with different sets of observations from 2000 to 2009
26 were conducted and optimized surface CO₂ fluxes from 2002 to 2009 were analyzed.

27 The global balances of the sources and sinks of surface CO₂ fluxes were maintained with a
28 similar trend for both experiments, while the distribution of the optimized surface CO₂ fluxes
29 changed. The magnitude of the optimized biosphere surface CO₂ uptake and its uncertainty in
30 EB (Siberia) was decreased from -1.17 ± 0.93 Pg C yr^{-1} to -0.77 ± 0.70 Pg C yr^{-1} , whereas it was
31 increased in other regions of the NH (Eurasian Temperate, Europe, North American Boreal,
32 and North American Temperate). The land sink of Europe increased significantly for 2008

1 and 2009, which is consistent with the other inversion results inferred by satellite observations.
2 Additional observations are used to correct the surface CO₂ uptake in June and July, the active
3 vegetation uptake season, in terms of monthly average optimized surface CO₂ fluxes. As a
4 result, the additional observations do not exhibit a change in the magnitude of the global
5 surface CO₂ flux balance because they provide detailed information about the Siberian land
6 sink instead of the global land sink magnitude, when they are used in the well-constructed
7 inversion modeling system.

8 The model CO₂ concentration using the background and optimized surface CO₂ fluxes in the
9 JR experiment are more consistent with the CO₂ observations used in the optimization than
10 those in the CNTL experiment, showing lower biases in the EB region. In contrast, the
11 differences of biases in ET and Europe between the two experiments are not distinguishable.
12 In comparison with vertical profiles of CO₂ concentration observations which are not used in
13 the optimization, the model CO₂ concentrations in the JR experiment show the smaller RMSD
14 and MAE, and the greater correlation coefficient than those in CNTL experiment.

15 The new observations provide useful information on the optimized surface CO₂ fluxes. The
16 observation impact of the Siberian observation data is investigated by means of uncertainty
17 reduction and self-sensitivity calculated by an influence matrix. Additional observations
18 reduce the uncertainty of the optimized surface CO₂ fluxes in Asia and Europe, mainly in the
19 EB (Siberia), where the new observations are used in the assimilation. The average self-
20 sensitivities of the JR-STATION sites are approximately 60% larger than those at other
21 continuous measurements (e.g., tower measurements in North America). The global average
22 self-sensitivity and cumulative impact of the JR experiment are higher than that of the CNTL
23 experiment, which implies that the individual observation impact of JR-STATION data on
24 optimized surface CO₂ fluxes is higher than the average values. The RMSD of the analyzed
25 surface CO₂ fluxes constrained by one week of observations from the background fluxes also
26 suggests that new Siberian observations provide a larger amount of information on the
27 optimized surface CO₂ fluxes.

28 This study shows that the JR-STATION data affect the longitudinal distribution of the total
29 NH sinks, especially in the EB and Europe, when it is used by atmospheric CO₂ inversion
30 modeling. In the future, it is expected that Siberian observations will be used as an important
31 constraint for estimating surface CO₂ fluxes over the NH with various CO₂ observations (e.g.
32 satellite and aircraft measurements) simultaneously.

1 **Acknowledgements**

2 The authors appreciate two reviewers for their valuable comments. This study was funded by
3 the Korea Meteorological Administration Research and Development Program under the
4 Grant KMIPA 2015-2021. The JR-STATION is supported by the Global Environment
5 Research Account for National Institutes of the Ministry of the Environment, Japan and the
6 Russian Foundation for Basic Research (Grant No. 14-05-00590). The authors also
7 acknowledge atmospheric CO₂ measurements data providers and cooperating agencies at
8 China Meteorological Administration, Commonwealth Scientific and Industrial Research
9 Organization, Environment Canada, Finnish Meteorological Institute, Hungarian
10 Meteorological Service, Japan Meteorological Agency, Lawrence Berkeley National
11 Laboratory, National Institute of Environmental Research, Norwegian Meteorological
12 Institute, Max Planck Institute for Biogeochemistry, Morski Instytut Rybacki, National Center
13 for Atmospheric Research, National Oceanic and Atmospheric Administration Earth System
14 Research Laboratory, and Romanian Marine Research Institute.
15

1 **References**

- 2 Berchet, A., Pison, I., Chevallier, F., Bousquet, P., Bonne, J.-L., and Paris, J.-D.: Objectified
3 quantification of uncertainties in Bayesian atmospheric inversions, *Geosci. Model. Dev.*, 8,
4 1525-1546, doi:10.5194/gmd-8-1525-2015, 2015a.
- 5 Berchet, A., Pison, I., Chevallier, F., Paris, J.-D., Bousquet, P., Bonne, J.-L., Arshinov, M. Y.,
6 Belan, B. D., Cressot, C., Davydov, D. K., Dlugokencky, E. J., Fofonov, A. V., Galanin, A.,
7 Lavrič, J., Machida, T., Parker, R., Sasakawa, M., Spahni, R., Stocker, B. D., and Winderlich,
8 J.: Natural and anthropogenic methane fluxes in Eurasia: a mesoscale quantification by
9 generalized atmospheric inversion, *Biogeosciences*, 12, 5393-5414, doi:10.5194/bg-12-5393-
10 2015, 2015b.
- 11 Boden, T., Marland, G., and Andres, R.: Global, regional, and national fossil-fuel CO₂
12 emissions, Carbon Dioxide Information Analysis Center, Oak Ridge National Laboratory, US
13 Department of Energy, Oak Ridge, Tenn., USA doi:10.3334/CDIAC/00001_V2010, 10, 2010.
- 14 Bruhwiler, L. M. P., Michalak, A. M., and Tans, P. P.: Spatial and temporal resolution of
15 carbon flux estimates for 1983-2002, *Biogeosciences*, 8, 1309-1331, doi:10.5194/bg-8-1309-
16 2011, 2011.
- 17 Ciais, P., Reichstein, M., Viovy, N., Granier, A., Ogée, J., Allard, V., Aubinet, M., Buchmann,
18 N., Bernhofer, Chr., Carrara, A., Chevallier, F., De Noblet, N., Friend, A. D., Friedlingstein,
19 P., Grünwald, T., Heinesch, B., Keronen, P., Knohl, A., Krinner, G., Loustau, D., Manca, G.,
20 Matteucci, G., Miglietta, F., Ourcival, J. M., Papale, D., Pilegaard, K., Rambal, S., Seufert, G.,
21 Soussana, J. F., Sanz, M. J., Schulze, E. D., Vesala, T., and Valentini, R.: Europe-wide
22 reduction in primary productivity caused by the heat and drought in 2003, *Nature*, 529-533,
23 doi:10.1038/natures03972, 2005.
- 24 Chevallier, F., Bréon, F.-M., and Rayner, P. J.: Contribution of the Orbiting Carbon
25 Observatory to the estimation of CO₂ sources and sinks: Theoretical study in a variational
26 data assimilation framework, *J. Geophys. Res. Atmos.*, 112, D09307,
27 doi:10.1029/2006JD007375, 2007.
- 28 Chevallier, F., Ciais, P., Conway, T. J., Aalto, T., Anderson, B. E., Bousquet, P., Brunke, E.
29 G., Ciattaglia, L., Esaki, Y., Fröhlich, M., Gomez, A., Gomez-Pelaez, A. J., Haszpra, L.,
30 Krummel, P. B., Langenfelds, R. L., Leuenberger, M., Machida, T., Maignan, F., Matsueda,
31 H., Morguí, J. A., Mukai, H., Nakazawa, T., Peylin, P., Ramonet, M., Rivier, L., Sawa, Y.,

1 Schmdit, M., Steele, L. P., Vay, S. A., Vermeulen, A. T., Wofsy, S., and Worthy, D.: CO₂
2 surface fluxes at grid point scale estimated from a global 21 year reanalysis of atmospheric
3 measurements, *J. Geophys. Res. Atmos.*, 115, D21307, doi 10.1029/2010jd013887, 2010.

4 Dolman, A. J., Shvidenko, A., Schepaschenko, D., Ciais, P., Tchepakova, N., Chen, T., van
5 der Molen, M. K., Belelli Marchesini, L., Maximov, T. C., Maksyutov, S., and Schulze, E.-
6 D.: An estimate of the terrestrial carbon budget of Russia using inventory-based, eddy
7 covariance and inversion methods, *Biogeosciences*, 9, 5323-5340, doi:10.5194/bg-9-5323-
8 2012, 2012.

9 Engelen, R. J., Denning, A. S., Gurney, K. R., and TransCom3 modelers: On error estimation
10 in atmospheric CO₂ inversions, *J. Geophys. Res.*, 107, 4635, doi:10.1029/2002JD002195,
11 2002.

12 European Commission: Joint Research Centre (JRC)/Netherlands Environmental Assessment
13 Agency (PBL): Emission Database for Global Atmospheric Research (EDGAR), release
14 version 4.0, 2009.

15 Feng, L., Palmer, P. I., Parker, R. J., Deutscher, N. M., Feist, D. G., Kivi, R., Morino, I. and
16 Sussmann, R.: Estimates of European uptake of CO₂ inferred from GOSAT XCO₂ retrievals:
17 sensitivity to measurement bias inside and outside Europe, *Atmos. Chem. Phys.*, 16, 1289-
18 1302, doi:10.5194/acp-16-1289-2016, 2016.

19 Gurney, K. R., Law, R. M., Denning, A. S., Rayner, P. J., Baker, D., Bousquet, P., Bruhwiler,
20 L., Chen, Y. H., Ciais, P., Fan, S., Fung, I. Y., Gloor, M., Heimann, M., Higuchi, K., John, J.,
21 Maki, T., Maksyutov, S., Masarie, K., Peylin, P., Prather, M., Pak, B. C., Randerson, J.,
22 Sarmiento, J., Taguchi, S., Takahashi, T., and Yuen, C. W.: Towards robust regional
23 estimates of CO₂ sources and sinks using atmospheric transport models, *Nature*, 415, 626–630,
24 2002.

25 Hayes, D. J., McGuire, A. D., Kicklighter, D. W., Gurney, K. R., Burnside, T. J., and Melillo,
26 J. M.: Is the northern high-latitude land-based CO₂ sink weakening?, *Global Biogeochem. Cy.*,
27 25, GB3018, doi:10.1029/2010GB003813, 2011.

28 Houghton, R. A., Butman, D., Bunn, A. G., Krankina, O. N., Schlesinger, P., and Stone, T.
29 A.: Mapping Russian forest biomass with data from satellites and forest inventories. *Environ.*
30 *Res. Lett.*, 2, 045032, doi:10.1088/1748-9326/2/4/045032, 2007.

- 1 Houtekamer, P. L., and Mitchell, H. L.: A sequential ensemble Kalman filter for atmospheric
2 data assimilation, *Mon. Wea. Rev.*, 129, 123-137, 2001.
- 3 Jacobson, A. R., Mikaloff Fletcher, S. E., Gruber, N., Sarmiento, J. L., and Gloor, M.: A joint
4 atmosphere–ocean inversion for surface fluxes of carbon dioxide: 1. Methods and global-scale
5 fluxes, *Global Biogeochem. Cy.*, 21, B1019, doi:10.1029/2005GB002556, 2007.
- 6 Kim, J., Kim, H. M., and Cho, C.-H.: Application of Carbon Tracking System based on
7 ensemble Kalman Filter on the diagnosis of Carbon Cycle in Asia, *Atmosphere*, 22(4), 415-
8 447, 2012. (in Korean with English abstract)
- 9 Kim, J., Kim, H. M., and Cho, C.-H.: The effect of optimization and the nesting domain on
10 carbon flux analyses in Asia using a carbon tracking system based on the ensemble Kalman
11 filter, *Asia-Pacific J. Atmos. Sci.*, 50, 327-344, doi:10.1007/s13143-014-0020-7, 2014a.
- 12 Kim, J., H. M. Kim, and C.-H. Cho, 2014b: Influence of CO₂ observations on the optimized
13 CO₂ flux in an ensemble Kalman filter, *Atmos. Chem. Phys.*, 14, 13515-13530,
14 doi:10.5194/acp-14-13515-2014, 2014b.
- 15 Knorr, W., Gobron, N., Scholze, M., Kaminski, T., Schnur, R., and Pinty, B.: Impact of
16 terrestrial biosphere carbon exchanges on the anomalous CO₂ increase in 2002-2003,
17 *Geophys. Res. Lett.*, 34, L09703, doi:10.1029/2006GL029019, 2007.
- 18 Krol, M., Houweling, S., Bregman, B., Broek, M., van der Segers, A., Velthoven, P. V.,
19 Peters, W., Dentener, F., and Bergamaschi, P.: The two-way nested global chemistry-
20 transport zoom model TM5: Algorithm and applications, *Atmos. Chem. Phys.*, 5, 417-432,
21 2005.
- 22 Kurganova, I. N., Kudeyarov, V. N., and Lopes De Gerenyu, V. O.: Updated estimate of
23 carbon balance on Russian territory, *Tellus*, 62B, 497-505, doi:10.1111/j.1600-
24 0889.2010.00467.x, 2010.
- 25 Le Quéré, C., Moriarty, R., Andrew, R. M., Peters, G. P., Ciais, P., Friedlingstein, P., Jones, S.
26 D., Sitch, S., Tans, P., Arneeth, A., Boden, T. A., Bopp, L., Bozec, Y., Canadell, J. G., Chini, L.
27 P., Chevallier, F., Cosca, C. E., Harris, I., Hoppema, M., Houghton, R. A., House, J. I., Jain,
28 A. K., Johannessen, T., Kato, E., Keeling, R. F., Kitidis, V., Klein Goldewijk, K., Koven, C.,
29 Landa, C. S., Landschützer, P., Lenton, A., Lima, I. D., Marland, G., Mathis, J. T., Metzl, N.,
30 Nojiri, Y., Olsen, A., Ono, T., Peng, S., Peters, W., Pfeil, B., Poulter, B., Raupach, M. R.,
31 Regnier, P., Rödenbeck, C., Saito, S., Salisbury, J. E., Schuster, U., Schwinger, J., Séférian,

1 R., Segschneider, J., Steinhoff, T., Stocker, B. D., Sutton, A. J., Takahashi, T., Tilbrook, B.,
2 van der Werf, G. R., Viovy, N., Wang, Y.-P., Wanninkhof, R., Wiltshire, A., and Zeng, N.:
3 Global carbon budget 2014, *Earth Syst. Sci. Data*, 7, 47–85, doi:10.5194/essd-7-47-2015,
4 2015.

5 Lloyd, J., Langenfelds, R. L., Francey, R. J., Gloor, M., Tchebakova, N. M., Zolotoukhine, D.,
6 Brand, W. A., Werner, R. A., Jordan, A., Allison, C. A., Zrazhewske, V., Shibistova, O., and
7 Schulze, E.-D.: A trace-gas climatology above Zotino, central Siberia, *Tellus*, 54B, 749-767,
8 2002.

9 Machida, T., Matsueda, H., Sawa, Y., Nakagawa, Y., Hirotani, K., Kondo, N., Goto, K.,
10 Nakazawa, T., Ishikawa, K., and Ogawa, T.: Worldwide Measurements of Atmospheric CO₂
11 and Other Trace Gas Species Using Commercial Airlines, *J. Atmos. Oceanic Techno.*, 25,
12 1744-1754, doi:10.1175/2008JTECHA1082.1, 2008.

13 Machida, T., Tohjima, Y., Katsumata, K., and Mukai, H.: A new CO₂ calibration scale based
14 on gravimetric one-step dilution cylinders in National Institute for Environmental Studies-
15 NIES 09 CO₂ scale, Report of the 15th WMO/IAEA Meeting of Experts on Carbon Dioxide,
16 Other Related Tracer Measurement Techniques, GAW Rep. 194, 165-169, World
17 Meteorological Organization, Geneva, Switzerland, 2011.

18 Maki, T., Ikegami, M., Fujita, T., Hirahara, T., Yamada, K., Mori, K., Takeuchi, A., Tsutsumi,
19 Y., Suda, K., and Conway, T. J.: New technique to analyse global distributions of CO₂
20 concentrations and fluxes from non-processed observational data, *Tellus*, 62B, 797-809,
21 doi:10.1111/j.1600-0889.2010.00488.x, 2010.

22 Maksyutov, S., Machida, T., Mukai, H., Patra, P. K., Nakazawa, T., Inoue, G., and Transcom-
23 3 Modelers: Effect of recent observations on Asia CO₂ flux estimates by transport model
24 inversions, *Tellus*, 55B, 522-529, 2003.

25 Masarie, K. A., Peters, W., Jacobson, A. R., and Tans, P. P.: ObsPack: a framework for the
26 preparation, delivery, and attribution of atmospheric greenhouse gas measurements, *Earth*
27 *Syst. Sci. Data*, 6, 375-384, doi:10.5194/essd-6-375-2014, 2014.

28 Miller, C. E., Crisp, D., DeCola, P. L., Olsen, S. C., Randerson, J. T., Michalak, A. M.,
29 Alkhaled, A., Rayner, P., Jacob, D. J., Suntharalingam, P., Jones, D. B. A., Denning, A. S.,
30 Nicholls, M. E., Doney, S. C., Pawson, S., Boesch, H., Connor, B. J., Fung, I. Y., O'Brien, D.
31 O., Salawitch, R. J., Sander, S. P., Sen, B., Tans, P., Toon, G. C., Wennberg, P. O., Wofsy, S.

1 C., Yung, Y. L., and Law, R. M.: Precision requirements for space-based XCO₂ data, *J.*
2 *Geophys. Res.*, 112, D10314, doi:10.1029/2006JD007659, 2007.

3 Olson, J., Watts, J., and Allsion, L.: Major World Ecosystem Complexes Ranked by Carbon
4 in Live Vegetation: a Database, Tech. rep., Carbon Dioxide Information Analysis Center, U.S.
5 Department of Energy, Oak Ridge National Laboratory, Oak Ridge, Tennessee, USA,
6 doi:10.3334/CDIAC/lue.ndp017, 1992.

7 Olsen, S. C., and Randerson, J. T.: Differences between surface and column atmospheric CO₂
8 and implications for carbon cycle research, *J. Geophys. Res.*, 109, D02301,
9 doi:10.1029/2003JD003968, 2004.

10 Paris, J.-D., Ciais, P., Nédélec, P., Ramonet, M., Belan, B. D., Arshinov, M. Y., Golitsyn, G.
11 S., Granberg, I., Stohl, A., Cayez, G., Athier, G., Boumard, F., and Cousin, J. M.: The YAK-
12 AEROSIB transcontinental aircraft campaigns: new insights on the transport of CO₂, CO and
13 O₃ across Siberia, *Tellus B*, 60, 551– 568, 2008.

14 Peters, W., Jacobson, A. R., Sweeney, C., Andrews, A. E., Conway, T. J., Masarie, K., Miller,
15 J. B., Bruhwiler, L. M. P., Petron, G., Hirsch, A. I., Worthy, D. E. J., van der Werf, G. R.,
16 Randerson, J. T., Wennberg, P. O., Krol, M. C., Tans, P. P.: An atmospheric perspective on
17 North American carbon dioxide exchange: CarbonTracker, *Proc. Nat. Acad. Sci. U.S.A.*, 104,
18 18925-18930, 2007.

19 Peters, W., Krol, M. C., van der Werf, G. R., Houweling, S., Jones, C. D., Hughes, J.,
20 Schaefer, K., Masarie, K. A., Jacobson, A. R. Miller, J. B., Cho, C. H., Ramonet, M., Schmidt,
21 M., Ciattaglia, L., Apadula, F., Heltai, D., Meinhardt, F., di Sarra, A. G., Piacentino, S.,
22 Sferlazzo, D., Aalto, T., Hatakka, J., Ström, J., Haszpra, L., Meijer, H. A. J., van der Laan, S.,
23 Neubert, R. E. M., Jordan, A., Rodó, X., Morguί, J. A., Vermeulen, A. T., Popa, E., Rozanski,
24 K., Zimnoch, M., Manning, A. C., Leuenberger, M., Uglietti, C., Dolman, A. J., Ciais, P.
25 Heimann, M., and Tans, P. P.: Seven years of recent European net terrestrial carbon dioxide
26 exchange constrained by atmospheric observations, *Global Change Biol.*, 16, 1317-1337,
27 doi:10.1111/j.1365-2486.2009.02078.x, 2010.

28 Peylin P., Law, R. M., Gurney, K. R., Chevallier, F., Jacobson A. R., Maki, T., Niwa, Y.,
29 Patra, P. K., Peters, W., Rayner, P. J., Rödenbeck, C., van der Laan-Luijkx, I. T., and Zhang,
30 X.: Global atmospheric carbon budget: results from an ensemble of atmospheric CO₂
31 inversions, *Biogeosciences*, 10, 6699-6720, doi:10.5194/bg-10-6699-2013, 2013.

1 Quegan, S., Beer, C., Shvidenko, A., McCallum, I., Handoh, I. C., Peylin, P., Rödenbeck, C.,
2 Lucht, W., Nilsson, S., and Schmullius, C.: Estimating the carbon balance of central Siberia
3 using landscape-ecosystem approach, atmospheric inversion and dynamic global vegetation
4 models, *Glob. Change Biol.*, 17, 351-365, doi:10.1111/j.1365-2486.2010.02275.x, 2011.

5 Reuter, M., Buchwitz, M., Hilker, M., Heymann, J., Schneising, O., Pillai, D., Bovensmann,
6 H., Burrows, J. P., Bösch, H., Parker, R., Butz, A., Hasekamp, O., O'Dell, C. W., Yoshida, Y.,
7 Gerbig, C., Nehr Korn, T., Deutscher, N. M., Warneke, T., Notholt, J., Hase, F., Kivi, R.,
8 Sussmann, R., Machida, T., Matsueda, H., and Sawa, Y.: Satellite-inferred European carbon
9 sink larger than expected, *Atmos. Chem. Phys.*, 14, 13739-13753, doi:10.5194/acp-14-13739-
10 2014, 2014.

11 Saeki, T., Maksyutov, S., Sasakawa, M., Machida, T., Arshinov, M., Tans, P. P., Conway, T.
12 J., Saito, M., Valsala, V., Oda, T., Andres, R. J., and Belikov, D.: Carbon flux estimation for
13 Siberia by inverse modeling constrained by aircraft and tower CO₂ measurements, *J. Geophys.*
14 *Res. Atmos.*, 118, 1100-1122, doi:10.1002/jgrd.50127, 2013.

15 Sasakawa, M., Shimoyama, K., Machida, T., Tsuda, N., Suto, H., Arshinov, M., Davydov, D.,
16 Fofonov, A., Krasnov, O., Saeki, T., Koyama, Y., and Maksyutov, S.: Continuous
17 measurements of methane from a tower network over Siberia, *Tellus*, 62B, 403-416,
18 doi:10.1111/j.1600-0889.2010.00494.x, 2010.

19 Sasakawa, M., Machida, T., Tsuda, N., Arshinov, M., Davydov, D., Fofonov, A., and
20 Krasnov, O.: Aircraft and tower measurements of CO₂ concentration in the planetary
21 boundary layer and the lower free troposphere over southern taiga in West Siberia: Long-term
22 records from 2002 to 2011, *J. Geophys. Res. Atmos.*, 118, 9489-9498,
23 doi:10.1002/jgrd.50755, 2013.

24 Schepaschenko, D., McCallum, I., Shvidenko, A., Fritz, S., Kraxner, F., and Obersteiner, M. :
25 A new hybrid land cover dataset for Russia: a methodology for integrating statistics, remote
26 sensing and in situ information, *J. Land Use Sci.*, 6, 245-259,
27 doi:10.1080/1747423X.2010.511681, 2011.

28 Schneising, O., Buchwitz, M., Reuter, M., Heymann, J., Bovensmann, H., and Burrows, J. P.:
29 Long-term analysis of carbon dioxide and methane column-averaged mole fractions retrieved
30 from SCIAMACHY, *Atmos. Chem. Phys.*, 11, 2863-2880, doi:10.5194/acp-11-2863-2011,
31 2011

1 Schulze, E.-D., Lloyd, J., Kelliher, F. M., Wirth, C., Reibmann, C., Lühker, B., Mund, M.,
2 Knohl, A., Milyukova, I. M., Schulze, W., Ziegler, W., Varlagin, A. B., Sogachev, A. F.,
3 Valentini, R., Dore, S., Grigoriev, S., Kolle, O., Panfyorov, M. I., Tchebakova, N., and
4 Vygodskaya, N. N.: Productivity of forests in the Euro Siberian boreal region and their
5 potential to act as a carbon sink – a synthesis. *Glob. Change Biol.*, 5, 703-722,
6 doi:10.1046/j.1365-2486.1999.00266.x, 1999.

7 Tarnocai, C., Canadell, J. G., Schuur, E. A. G., Kuhry, P., Mazhitova, G., and Zimov, S.: Soil
8 organic carbon pools in the northern circumpolar permafrost region, *Glob. Biogeochem.*
9 *Cycles*, 23, GB2023, doi:10.1029/2008GB003327, 2009.

10 Turnbull, J. C., Miller, J. B., Lehman, S. J., Hurst, D., Peters, W., Tans, P. P., Southon, J.,
11 Montzka, S. A., Elkins, J. W., Mondeel, D. J., Romashkin, P. A., Elansky, N., and
12 Skorokhod, A.: Spatial distribution of $\Delta^{14}\text{CO}_2$ across Eurasia: measurements from the
13 TROICA-8 expedition, *Atmos. Chem. Phys.*, 9, 175-187, doi:10.5194/acp-9-175-2009, 2009.

14 van der Laan-Luijkx, I. T., van der Velde, I. R., Krol, M. C., Gatti, L. V., Domingues, L. G.,
15 Correia, C. S. C., Miller, J. B., Gloor, M., van Leeuwen, T. T., Kaiser, J. W., Wiedinmyer, C.,
16 Basu, S., Clerbaux, C., and Peters, W.: Response of the Amazon carbon balance to the 2010
17 drought derived with CarbonTracker South America, *Global Biogeochem. Cycles*, 29, 1092-
18 1108, doi:10.1002/2014GB005082, 2015.

19 van der Werf, G. R., Randerson, J. T., Giglio, L., Collatz, G. J., Mu, M., Kasibhatla, P. S.,
20 Morton, D. C., DeFries, R. S., Jin, Y., and van Leeuwen, T. T.: Global fire emissions and the
21 contribution of deforestation, savanna, forest, agricultural, and peat fires (1997–2009), *Atmos.*
22 *Chem. Phys.*, 10, 11707–11735, doi:10.5194/acp-10-11707-2010, 2010.

23 Whitaker, J. S., and Hamill, T. M.: Ensemble Data Assimilation without Perturbed
24 Observations, *Mon. Wea. Rev.*, 130, 1913-1924, 2002.

25 Winderlich, J., Chen, H., Gerbig, C., Seifert, T., Kolle, O., Lavrič, Kaier, C., Höfer, A., and
26 Heimann, H.: Continuous low-maintenance $\text{CO}_2/\text{CH}_4/\text{H}_2\text{O}$ measurements at the Zotino Tall
27 Tower Observatory (ZOTTO) in Central Siberia, *Atmos. Meas. Tech.*, 3, 1113-1128,
28 doi:10.5194/amt-3-1113-2010, 2010.

29 Zhang, H. F., Chen, B. Z., van der Laan-Luijkx, I. T., Chen, J., Xu, G., Yan, J. W., Zhou, L.
30 X., Fukuyama, Y., Tans, P. P., and Peters, W.: Net terrestrial CO_2 exchange over China

1 during 2001–2010 estimated with an ensemble data assimilation system for atmospheric CO₂.
2 J. Geophys. Res. Atmos., 119, 2013JD021297, doi:10.1002/2013JD021297, 2014a.
3 Zhang, H. F, Chen, B. Z., van der Laan-Luijkx, Machida, T., Matsueda, H., Sawa, Y,
4 Fukuyama, Y., Labuschagne, C., Langenfelds, R., van der Schoot, M., Xu, G., Yan, J. W.,
5 Zhou, L. X., Tans, P. P., and Peters, W.: Estimating Asian terrestrial carbon fluxes from
6 CONTRAIL aircraft and surface CO₂ observations for the period 2006 to 2010, Atmos. Chem.
7 Phys., 14, 5807-5824, doi:10.5194/acp-14-7807-2014, 2014b.
8

1 Table 1. Information on observation sites located in the Asia and Europe region. MDM
 2 represents the model-data mismatch which is the observation error.

Site	Location	Latitude	Longitude	Height (Sampling height) (m)	Laboratory (Cooperating agency)	MDM (ppm)
AZV	Azovo, Russia	54.71°N	73.03°E	110(50)	NIES	3
BRZ	Berezorechka, Russia	56.15°N	84.33°E	168(80)	NIES	3
DEM	Demyanskoe, Russia	59.79°N	70.87°E	63(63)	NIES	3
IGR	Igrim, Russia	63.19°N	64.41°E	9(47)	NIES	3
KRS	Karasevoe, Russia	58.25°N	82.42°E	76(67)	NIES	3
NOY	Noyabrsk, Russia	63.43°N	75.78°E	108(43)	NIES	3
SVV	Savvushka, Russia	51.33°N	82.13°E	495(52)	NIES	3
VGN	Vaganovo, Russia	54.50°N	62.32°E	192(85)	NIES	3
YAK	Yakutsk, Russia	62.09°N	129.36°E	264(77)	NIES	3
WLG	Mt. Waliguan, China	36.29°N	100.9°E	3810	CMA/ESRL	1.5
BKT	Bukit Kototabang, Indonesia	0.20°S	100.32°E	864	ESRL	7.5
WIS	Sede Boker, Israelr,	31.13°N	34.88°E	400	ESRL	2.5
KZD	Sary Taukum, Kazakhstan	44.45°N	77.57°E	412	ESRL	2.5
KZM	Plateau Assy, Kazakhstan	43.25°N	77.88°E	2519	ESRL	2.5
TAP	Tae-ahn Peninsula, South Korea	36.73°N	126.13°E	20	ESRL	5
UUM	Ulaan Uul, Mongolia	44.45°N	111.10°E	914	ESRL	2.5
CRI	Cape Rama, India	15.08°N	73.83°E	60	CSIRO	3
LLN	Lulin, Taiwan	23.47°N	120.87°E	2862	ESRL	7.5
SDZ	Shangdianzi, China	40.39°N	117.07°E	287	CMA/ESRL	3
MNM	Minamitorishima, Japan	24.29°N	153.98°E	8	JMA	3
RYO	Ryori, Japan	39.03°N	141.82°E	260	JMA	3
YON	Yonagunijima, Japan	24.47°N	123.02°E	30	JMA	3
GSN	Gosan, South Korea	33.15°N	126.12°E	72	NIER	3
BAL	Baltic Sea, Poland	55.35°N	17.22°E	3	ESRL (MIR*)	7.5
BSC	Black Sea, Constanta, Romania	44.17°N	28.68°E	3	ESRL (RMRI*)	7.5
HUN	Hegyhatsal, Hungary	46.95°N	16.65°E	248	ESRL (HMS*)	7.5
OBN	Obninsk, Russia	55.11°N	36.60°E	183	ESRL	7.5
OXK	Ochsenkopf, Germany	50.03°N	11.80°E	1022	ESRL (MPI-BGC*)	2,5
PAL	Pallas-Sammaltunturi, GaW Station, Finland	67.97°N	24.12°E	560	ESRL (FMI*)	2.5
STM	Ocean Station M, Norway	66.00°N	2.00°E	0	ESRL (MET Norway*)	1.5

3 * Cooperating agencies of observation sites in Euope: Morski Instytut Rybacki (MIR), Romanian Marine
 4 Research Institute (RMRI), Hungarian Meteorological Service (HMS), Max Plnack Institute for
 5 Biogeochemistry (MPI-BGC), Finnish Meteorological Institute (FMI), Norwegian Meteorological Institute
 6 (MET Norway).

1 Table 2. A prior and optimized surface CO₂ fluxes and their one-sigma uncertainties (Pg C
 2 yr⁻¹ Region⁻¹) of global total, land, ocean, and other regions averaged spatially from 2002 to
 3 2009.

Region	A priori	CNTL	JR.
Eurasian Boreal	-0.07±1.10	-1.17±0.93	-0.77±0.70
Eurasian Temperate	-0.05±0.49	-0.31±0.41	-0.36±0.40
Europe	-0.01±-0.76	-0.20±0.67	-0.37±0.64
North American Boreal	-0.04±0.61	-0.30±0.38	-0.36±0.38
North American Temperate	-0.02±0.66	-0.55±0.41	-0.59±0.41
Northern Hemisphere total	-1.42±1.85	-3.21±1.49	-3.21±1.34
Tropical total	0.06±0.80	0.12±0.74	0.11±0.74
Southern Hemisphere total	-2.57±0.97	-2.46±0.81	-2.45±0.81
Global total	-3.94±2.24	-5.54±1.85	-5.55±1.72
Global land	-1.33±1.90	-3.59±1.57	-3.52±1.43
Global ocean	-2.61±1.19	-1.95±0.97	-2.03±0.96

1 Table 3. The optimized surface CO₂ fluxes (Pg C yr⁻¹ Region⁻¹) of ecosystem types at Eurasian Boreal, Eurasian Temperate, Europe, North
 2 American Boreal, and North American Temperate region averaged over 2002 - 2009.

Ecosystem type	Eurasian Boreal		Eurasian Temperate		Europe		North American Boreal		North American Temperate	
	CNTL	JR	CNTL	JR	CNTL	JR	CNTL	JR	CNTL	JR
Conifer Forest	-0.815	-0.337	-0.005	-0.005	-0.067	-0.069	-0.107	-0.121	-0.054	-0.069
Broadleaf Forest	-0.006	-0.013	-0.004	-0.005	-0.005	-0.005	0.000	0.000	-0.002	-0.002
Mixed Forest	-0.049	-0.090	-0.029	-0.034	-0.025	-0.063	-0.053	-0.054	-0.019	-0.021
Grass/Shrub	-0.035	-0.056	-0.247	-0.285	-0.016	-0.032	0.000	-0.001	-0.077	-0.081
Tropical Forest	0.000	0.000	-0.001	-0.001	0.000	0.000	0.000	0.000	0.000	0.000
Scrub/Woods	0.000	0.000	-0.002	-0.002	-0.001	-0.001	0.000	0.000	-0.013	-0.013
Semitundra	-0.145	-0.188	-0.007	-0.009	-0.008	-0.009	-0.057	-0.086	-0.010	-0.011
Fields/Woods/Savanna	-0.012	-0.021	-0.005	-0.005	0.003	-0.009	-0.004	-0.004	-0.149	-0.153
Northern Taiga	-0.094	-0.029	0.000	0.000	-0.006	-0.007	-0.066	-0.077	0.000	0.000
Forest/Field	-0.003	-0.008	0.006	0.006	-0.086	-0.105	-0.001	-0.001	-0.012	-0.016
Wetland	-0.002	-0.014	0.000	-0.000	-0.001	-0.002	-0.003	-0.006	-0.002	-0.003
Shrub/Tree/Suc	0.000	0.000	-0.001	-0.001	0.000	0.000	0.000	0.000	0.000	0.000
Crops	-0.002	-0.008	-0.019	-0.022	-0.007	-0.075	0.000	0.000	-0.216	-0.227
Wooded tundra	-0.003	-0.005	0.000	0.000	0.003	0.003	-0.003	-0.002	0.000	0.000
Water	0.000	0.000	0.000	0.000	0.000	0.000	-0.001	-0.001	-0.001	-0.001

1 Table 4. Average differences between: model CO₂ concentrations (ppm) simulated using the
 2 background and the observed CO₂ concentration (ppm) (fourth and sixth columns), model
 3 CO₂ concentrations (ppm) simulated using the optimized surface CO₂ flux and the observed
 4 CO₂ concentration (ppm) (fifth and seventh columns), and average innovation χ^2 from 2002 to
 5 2009 at observation sites located in Asia and Europe (eighth column).

Region	Site	MDM [ppm]	CNTL		JR		Innovation χ^2
			Bias (background)	Bias (optimized)	Bias (background)	Bias (optimized)	
Eurasian	AZV	3	1.68	1.04	0.77	0.19	0.85
Boreal	BRZ	3	1.41	0.68	0.67	0.39	1.17
	DEM	3	0.15	-0.84	0.32	0.11	0.84
	IGR	3	-1.58	-2.71	-0.52	-1.26	1.15
	KRS	3	0.57	-0.22	0.27	0.12	1.22
	NOY	3	-0.02	-1.06	0.16	0.00	0.86
	SVV	3	1.25	0.71	0.63	0.09	0.96
	VGN	3	2.55	2.11	1.50	0.84	1.18
	YAK	3	0.23	-2.18	0.87	0.03	1.36
Eurasian	WLG	1.5	0.17	0.19	0.15	0.16	1.09
Temperate	BKT	7.5	4.12	4.06	4.13	4.05	0.57
	WIS	2.5	0.27	0.12	0.22	0.07	0.72
	KZD	2.5	1.79	0.98	1.42	1.14	1.26
	KZM	2.5	1.17	0.96	1.13	0.93	1.26
	TAP	5	0.50	0.55	0.58	0.71	0.58
	UUM	2.5	0.24	-0.07	0.20	0.12	1.05
	CRI	3	-1.95	-1.57	-1.94	-1.56	0.66
	LLN	7.5	4.42	3.09	4.42	3.09	0.47
	SDZ	3	-3.02	-5.26	-3.09	-5.28	2.08
	MNM	3	0.56	0.52	0.59	0.56	0.17
	RYO	3	1.26	1.16	1.32	1.32	1.07
	YON	3	1.10	0.98	1.14	1.07	0.56
GSN	3	-1.92	-1.71	-1.92	-1.70	1.83	
Europe	BAL	7.5	-1.23	-1.32	-1.31	-1.45	0.37
	BSC	7.5	-4.12	-4.97	-4.12	-5.13	1.01
	HUN	7.5	0.93	0.53	0.86	0.36	0.46
	OBN	7.5	0.70	-0.71	0.59	-0.89	0.44
	OXK	2.5	0.50	0.02	0.43	-0.09	1.52
	PAL	2.5	0.47	0.07	0.58	0.16	0.76
	STM	1.5	0.54	0.42	0.55	0.42	0.76

6

1 Table 5. Bias, root mean square difference, mean absolute error, and Pearson's Correlation
 2 Coefficient of the model CO₂ concentration of CNTL and JR experiments in comparison with
 3 the vertical profile of CO₂ concentrations at BRZ site.

Altitude (km)	Bias (ppm)		Root-Mean-Square Difference (ppm)		Mean Absolute Error (ppm)		Pearson's Correlation Coefficient	
	CNTL	JR	CNTL	JR	CNTL	JR	CNTL	JR
~ 0.5	-0.13±4.81	0.20±4.57	4.82	4.57	3.45	3.23	0.95	0.95
0.5 ~ 1.0	0.58±4.30	0.83±4.10	4.34	4.18	3.14	3.03	0.95	0.95
1.0 ~ 1.5	0.40±3.94	0.56±3.69	3.96	3.74	2.88	2.68	0.93	0.94
1.5 ~ 2.0	0.25±3.46	0.42±3.24	3.47	3.27	2.49	2.34	0.93	0.94
2.0 ~ 2.5	0.43±3.20	0.59±2.91	3.22	2.97	2.35	2.18	0.92	0.94
2.5 ~ 3.0	0.56±2.89	0.73±2.58	2.94	2.69	2.21	2.08	0.90	0.92
3.0 ~	0.13±3.19	0.44±2.65	3.19	2.68	3.89	2.03	0.86	0.90

4

5

1 Table 6. Optimized surface CO₂ fluxes (Pg C yr⁻¹) from this study and other inversion studies.

Citation	Area	Estimate surface CO ₂ flux	Period	Remarks
This study	Eurasian Boreal	-0.77±0.70	2002-2009	JR experiment
Saeki et al. (2013)	Eurasian Boreal	-0.35±0.61	2000-2009	Including biomass burning (0.11Pg C yr ⁻¹), Using JR-STATION observations
Zhang et al. (2014b)	Eurasian Boreal	-1.02±0.91	2006-2010	Using CONTRAL observations
Maki et al. (2010)	Eurasian Boreal	-1.46±0.41	2001-2007	
Dolman et al. (2012)	Russia ^a	-0.613		Average of inventory-based, eddy covariance, and inversion methods
CT2013B ^b	Eurasian Boreal	-1.00±3.75	2002-2009	
This study	Europe	-0.38±0.64	2002-2009	JR experiment
Reuter et al. (2014)	Europe	-0.75±0.63	2008-2009	
		-1.02±0.30	2010	Using satellite data
CTE2014 ^c	Europe	-0.07±0.49	2002-2009	
		-0.11±0.38	2008-2009	

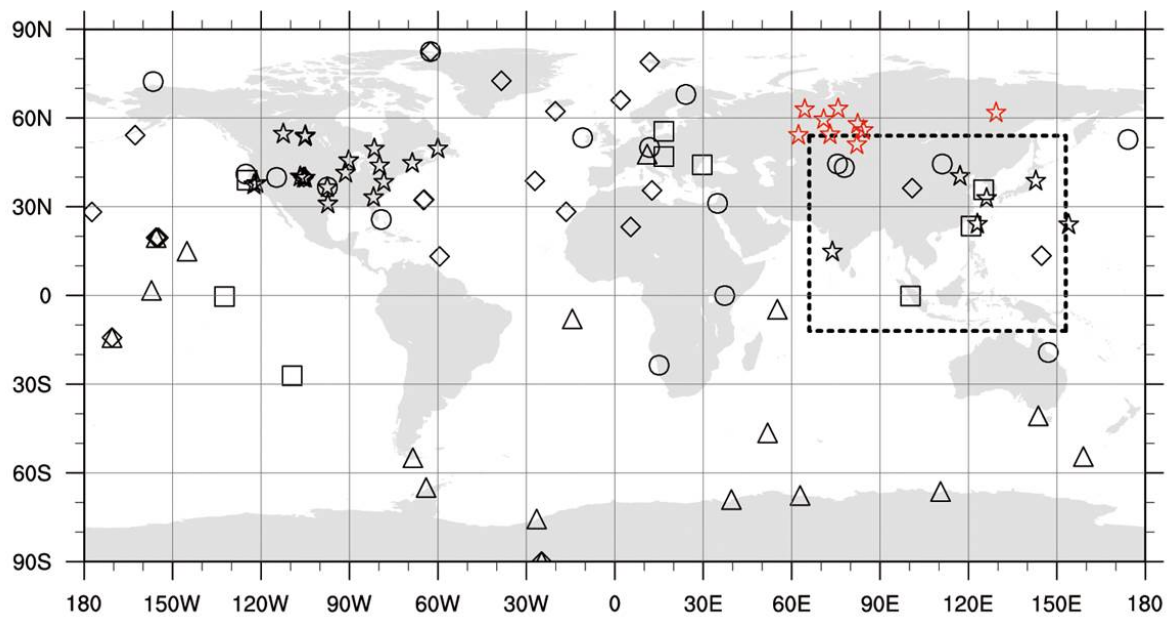
2 ^aIncluding Ukraine, Belarus and Kazakhstan (total area is 17.1×10¹² m²)

3 ^bThe results of CT2013B (<http://www.esrl.noaa.gov/gmd/ccgg/carbontracker/CT2013B/>) were
4 derived from (<ftp://aftp.cmdl.noaa.gov/products/carbontracker/co2/fluxes/>).

5 ^cThe results of CTE2014 (CarbonTracker Europe, Peters et al., 2010) were derived from
6 (<ftp://ftp.wur.nl/carbontracker/data/fluxes/>).

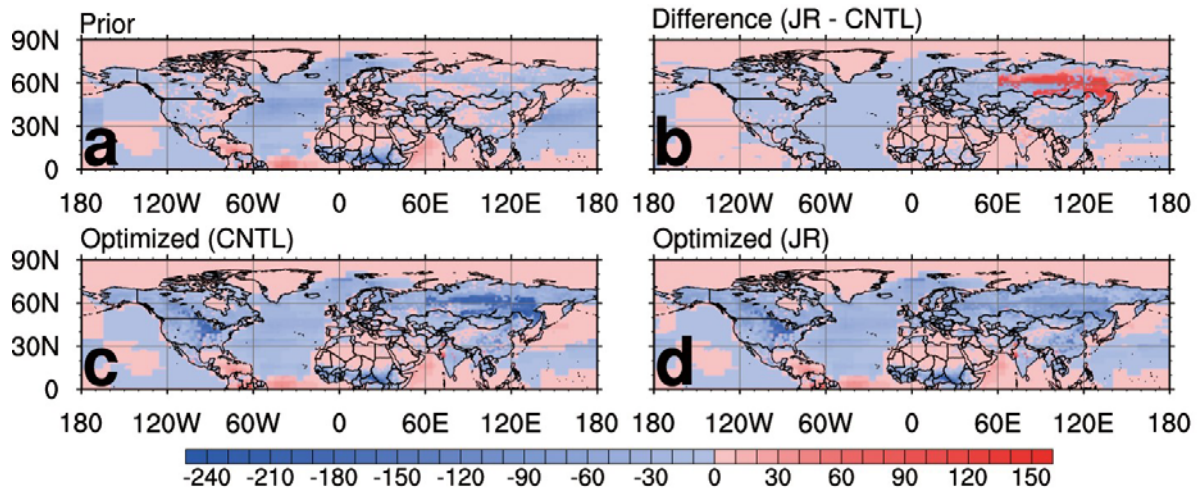
7

8



1
2
3
4
5
6
7

Figure 1. Observation networks of CO₂ concentrations around the globe and the nested domain of the TM5 transport model over Asia (dashed box). Each observation site is assigned to different categories (Δ : MBL; \circ : Continental; \diamond : Mixed land/ocean and mountain; \star : Continuous; \square : Difficult). JR-STATION observation sites are represented in red color.



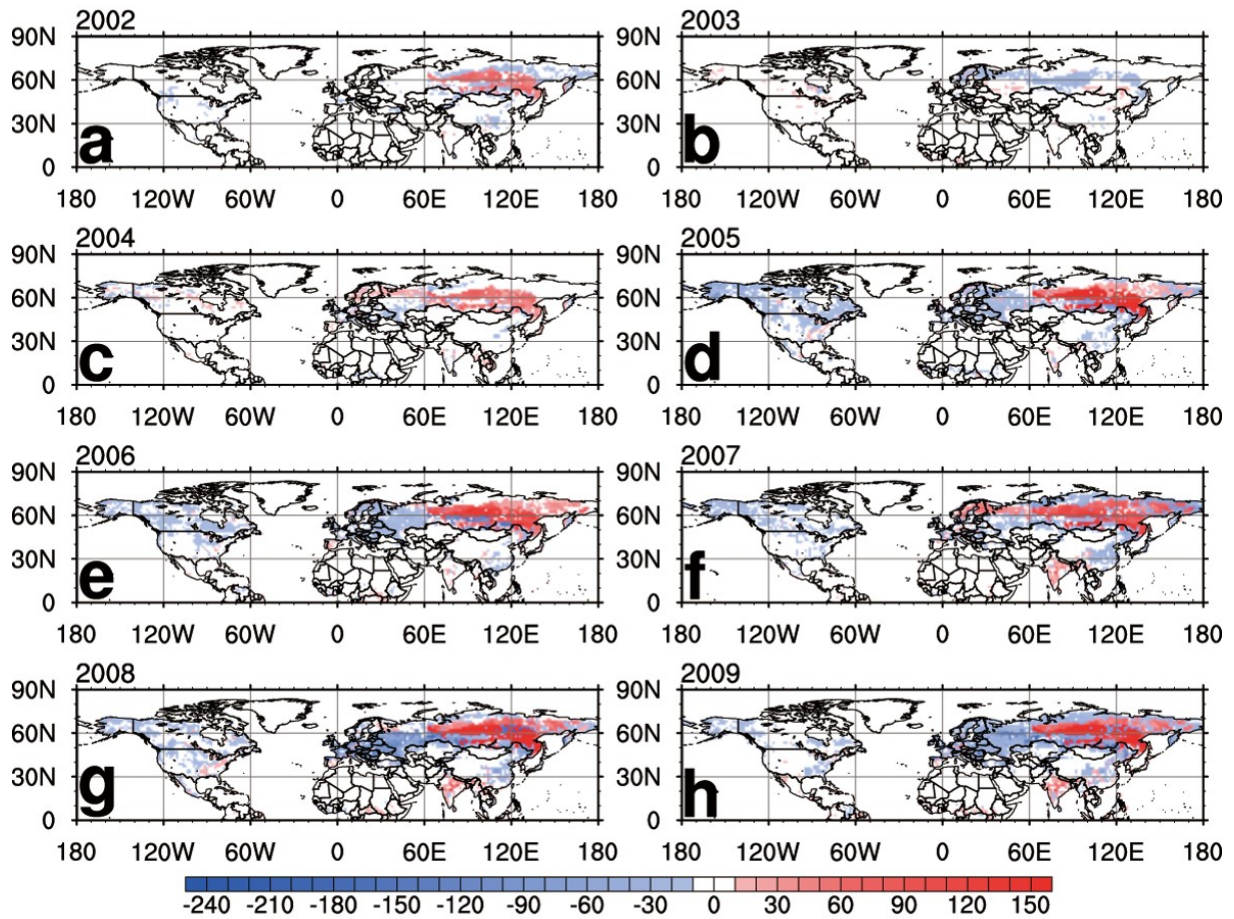
1

2

3 Figure 2. Average biosphere and ocean fluxes ($\text{gC m}^{-2} \text{yr}^{-1}$) from 2002 to 2009 of (a) the prior
 4 flux, (b) the difference between the optimized fluxes in the JR and CNTL experiments, (c) the
 5 optimized flux in the CNTL experiment, and (d) the optimized flux in the JR experiment.
 6 Blue colors (negative) denote net CO₂ flux uptake while red colors (positive) denote net CO₂
 7 release to the atmosphere. The difference is calculated by subtracting surface CO₂ flux of
 8 CNTL experiment from that of JR experiment.

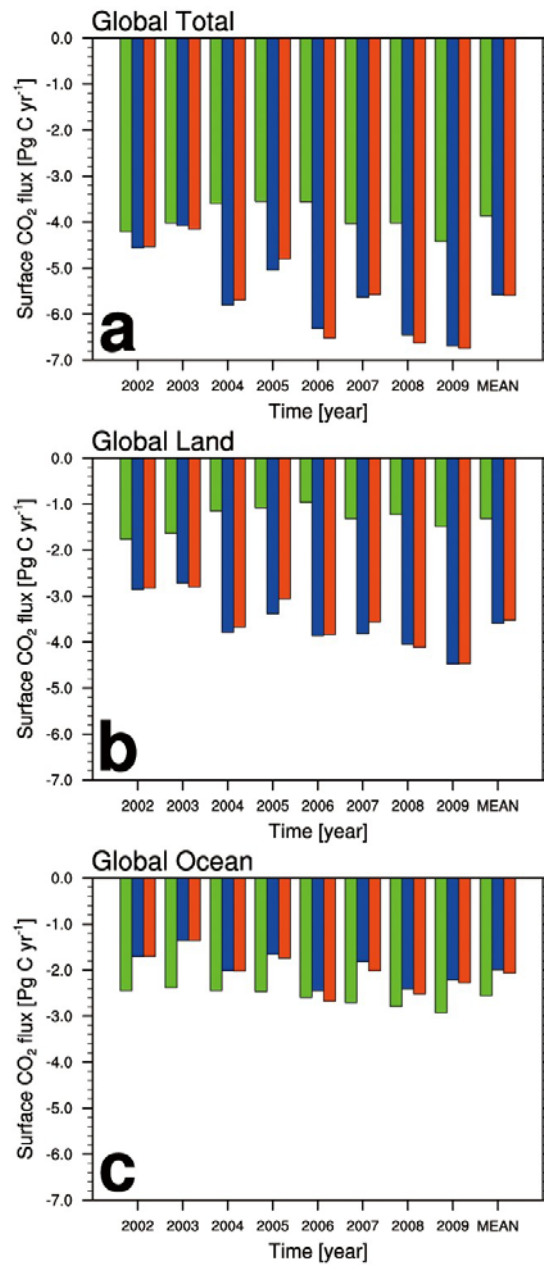
9

10



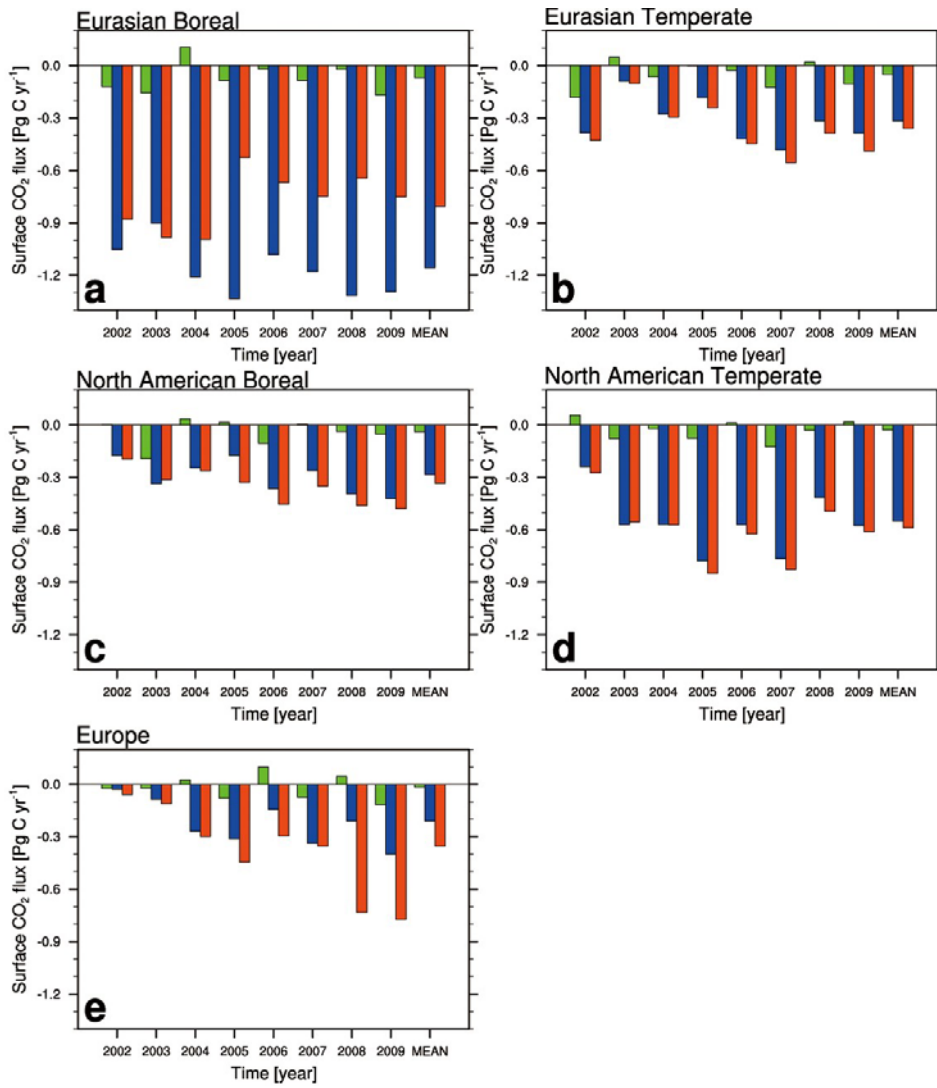
1
2
3
4
5
6
7
8
9

Figure 3. The difference between the optimized biosphere fluxes from the JR and CNTL experiment ($\text{g C m}^{-2} \text{ yr}^{-1}$) of (a) 2002, (b) 2003, (c) 2004, (d) 2005, (e) 2006, (f) 2007, (g) 2008, and (h) 2009. Blue colors (negative) denote net CO₂ flux uptake while red colors (positive) denote net CO₂ release to the atmosphere. The difference is calculated by subtracting surface CO₂ flux of CNTL experiment from that of JR experiment.



1
2
3
4
5
6

Figure 4. Annual and average biosphere and ocean fluxes (Pg C yr⁻¹) from the prior (green bar), CNTL (blue bar) and JR (red bar) experiment aggregated over the (a) whole globe, (b) land, and (c) ocean.

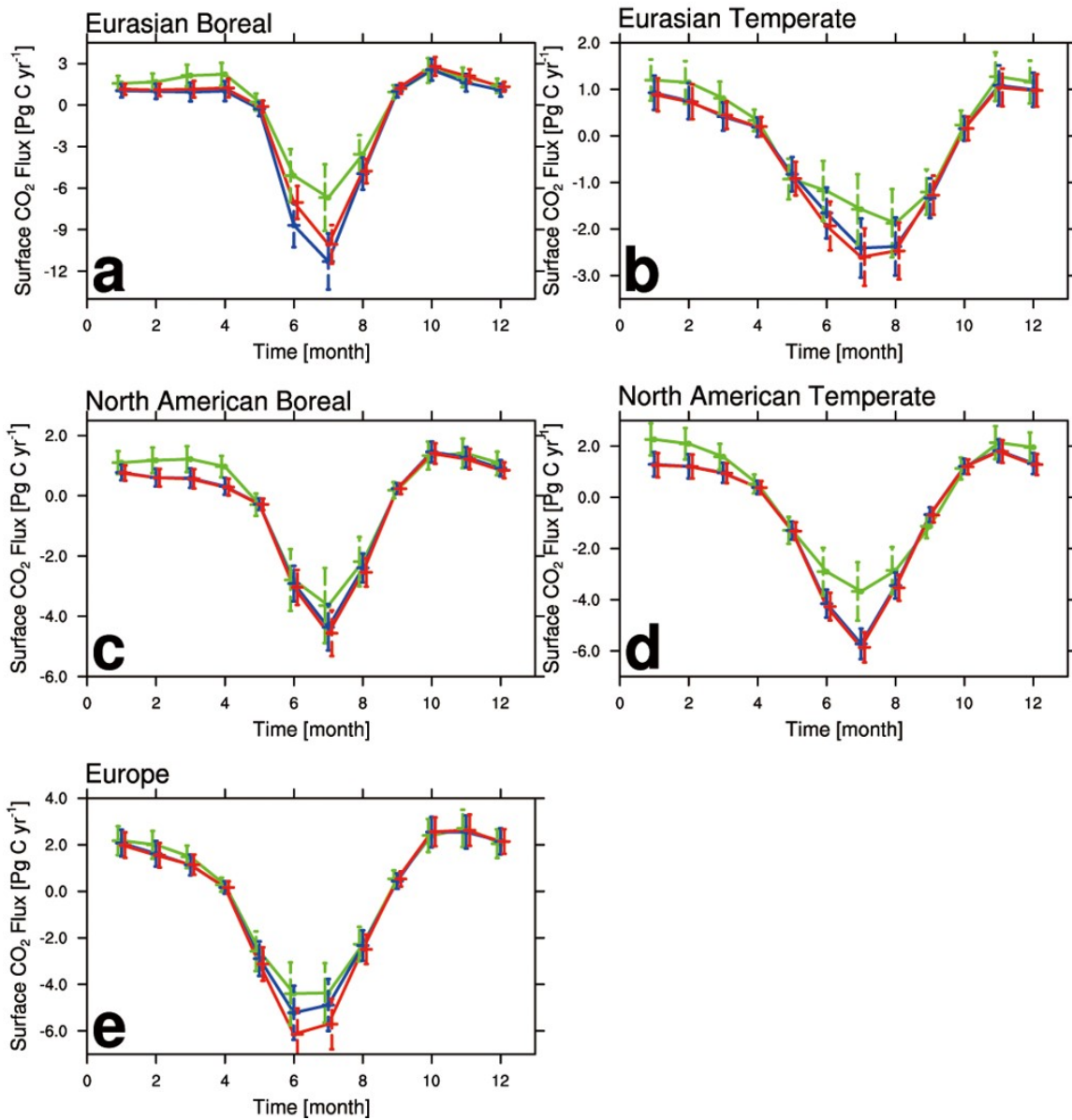


1

2 Figure 5. Annual and average biosphere fluxes (Pg C yr⁻¹) from the prior (green bar), CNTL
 3 (blue bar) and JR (red bar) experiment aggregated over the (a) Eurasian Boreal, (b) Eurasia
 4 Temperate, (c) North American Boreal, (d) North American Temperate, and (e) Europe.

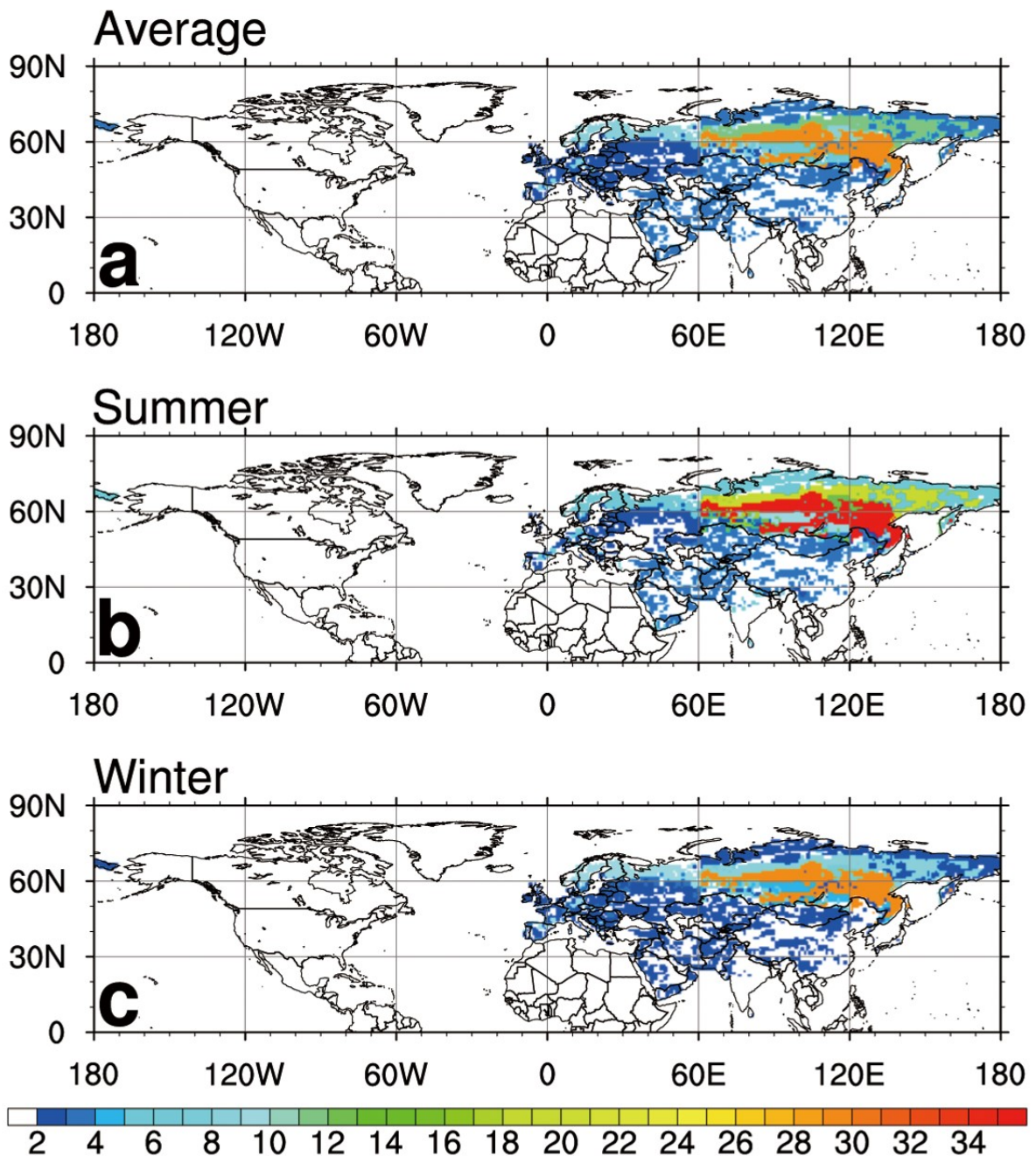
5

6



1
2
3
4
5
6
7

Figure 6. The monthly prior (green) and optimized biosphere fluxes averaged from 2002 to 2009 of CNTL (blue) and JR (red) experiment with their uncertainties over the (a) Eurasian Boreal, (b) Eurasian Temperate, (c) North American Boreal, (d) North American Temperate, and (e) Europe.



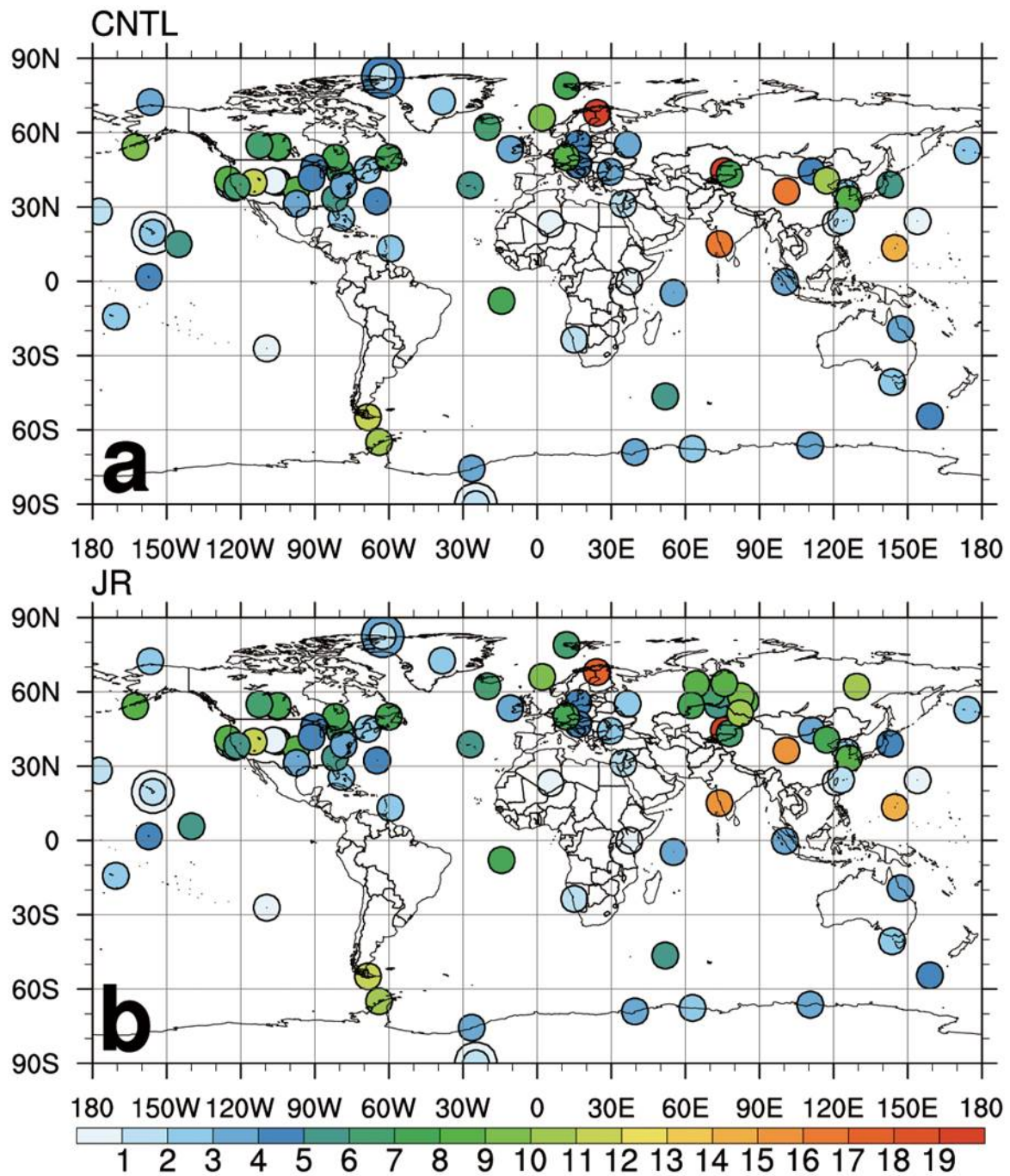
1

2

3 Figure 7. (a) Average uncertainty reduction (%) from 2002 to 2009, average uncertainty
 4 reduction (%) in (b) summer, and (c) winter for the estimated uncertainty of the JR
 5 experiment relative to that of the CNTL experiment. Red (blue) denotes relatively high (low)
 6 value of uncertainty reduction.

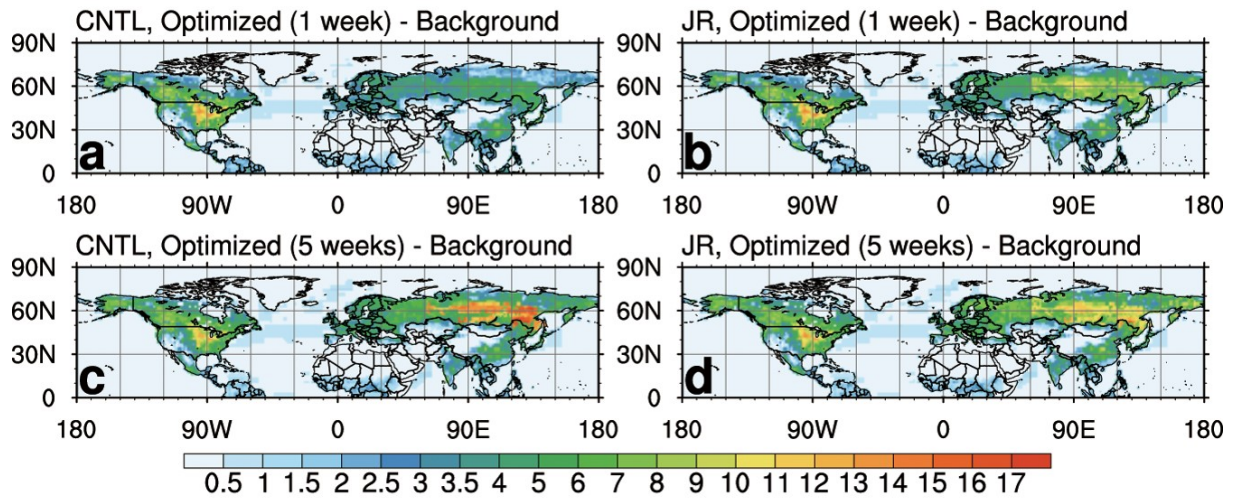
7

8



1
2
3
4
5
6
7

Figure 8. Self-sensitivity at each observation site averaged from 2002 to 2009 of (a) CNTL experiment and (b) JR experiment. The overlapping observation sites at the same locations or at close locations are distinguished by different sizes of circles. Red (blue) denotes relatively high (low) value of self-sensitivity.



1

2

3 Figure 9. RMSD averaged from 2002 to 2009 between the background flux and posterior flux
 4 optimized in Northern Hemisphere summer by 1 week of observations of (a) CNTL and (b)
 5 JR experiment; and by 5 weeks of observations of (c) CNTL and (d) JR experiment. The units
 6 are $\text{g C m}^{-2} \text{ week}^{-1}$. Red (blue) denotes relatively high (low) value of RMSD.